REPUBLIC OF TURKEY

GAZİANTEP UNIVERSITY

GRADUATE SCHOOL OF NATURAL & APPLIED SCIENCES

EXPERIMENTAL INVESTIGATION ON INFLUENCE OF PRINTING PARAMETERS ON MECHANICAL BEHAVIORS OF 3D PRINTED PARTS

M.Sc. THESIS

IN

MECHANICAL ENGINEERING

BY

BEYZA TOKLU

JANUARY 2022

JANUARY 2022

M.Sc. in Mechanical Engineering

BEYZA TOKLU

EXPERIMENTAL INVESTIGATION ON INFLUENCE OF PRINTING PARAMETERS ON MECHANICAL BEHAVIORS OF 3D PRINTED PARTS

M.Sc. Thesis

in

Mechanical Engineering

Gaziantep University

Supervisor

Assoc. Prof. Dr. Ömer Yavuz BOZKURT

Co-Supervisor

Dr. Özkan ÖZBEK

by

Beyza TOKLU

January 2022

I hereby declare that all information in this document has been obtained and presented in accordance with academic rules and ethical conduct. I also declare that, as required by these rules and conduct, I have fully cited and referenced all material and results that are not original to this work.

Beyza TOKLU

ABSTRACT

EXPERIMENTAL INVESTIGATION ON INFLUENCE OF PRINTING PARAMETERS ON MECHANICAL BEHAVIORS OF 3D PRINTED PARTS

TOKLU, Beyza
M.Sc. in Mechanical Engineering
Supervisor: Assoc. Prof. Dr. Ömer Yavuz BOZKURT
Co-Supervisor: Dr. Özkan ÖZBEK
January 2022
70 pages

This study aimed to investigate the effects of production parameters on mechanical properties of the parts that are produced using Polyethylene Terephthalate (PETG) filament in Fused Deposition Modeling (FDM) technique. For this purpose, a 3-axis 3D printer was used to fabricate the samples. The samples were fabricated at five different infill ratios (%20, %40, %60, %80, %100) and eight different infill patterns (Archimedes, 3D Honeycomb, Octogram Spiral, Gyroid, Triangle, Rectilinear, Honeycomb, Concentric). Uniaxial tensile and three-point bending experiments were performed to analyze mechanical responses of the samples, in accordance with ASTM D638 and ASTM D790 international standards, respectively. Additionally, the damaged samples were examined to understand fracture mechanisms. The results showed that the examined parameters had remarkable effects on mechanical behaviors. The increment in infill ratio led to increase in the strength of samples as a result of increase in the material amount. The Concentric pattern exhibited the highest tensile strength and flexural strength found as 49.82 MPa and 77.37 MPa at 100% infill ratio, respectively. However, the lowest tensile strength was obtained from the Triangle pattern with 13.77 MPa at 20% infill, and the lowest flexural strength was obtained from the 3D Honeycomb pattern at 20% infill. The results demonstrated the printing parameters for the parts fabricated using PETG filaments should be carefully chosen.

Key Words: 3D Printer, FDM, PETG, Infill Pattern, Infill Ratio.

ÖZET

BASKI PARAMETRELERININ 3B BASKILI PARÇALARIN MEKANIK DAVRANIŞLARINA ETKISI ÜZERINE DENEYSEL ARAŞTIRMA

TOKLU, Beyza
Yüksek Lisans Tezi, Makine Mühendisliği
Danışman: Doç. Dr. Ömer Yavuz BOZKURT
İkinci Danışman: Dr. Özkan ÖZBEK
Ocak 2022
70 sayfa

Bu çalışma, Polietilen Tereftalat (PETG) filamenti kullanılarak Eriyik Yığma Modelleme (FDM) tekniği ile üretilen parçaların mekanik özelliklerine üretim parametrelerinin etkilerini araştırmayı amaçlamıştır. Bu amaçla, numuneleri üretmek için 3 eksenli bir 3D yazıcı kullanıldı. Numuneler beş farklı dolgu oranında (%20, %40, %60, %80, %100) ve sekiz farklı dolgu deseninde (Arşimet, 3B Bal Peteği, Oktogram, Spiral, Gyroid, Üçgen, Doğrusal, Bal Peteği, Eş merkezli) üretilmiştir. Numunelerin mekanik tepkilerini analiz etmek için sırasıyla ASTM D638 ve ASTM D790 uluslararası standartlarına göre tek eksenli çekme ve üç nokta eğilme deneyleri yapılmıştır. Ek olarak, kırılma mekanizmalarını anlamak için hasarlı numuneler incelenmiştir. Sonuçlar, incelenen parametrelerin mekanik davranışlar üzerinde dikkate değer etkileri olduğunu göstermiştir. Dolgu oranındaki artış, malzeme miktarının artması sonucu numunelerin mukavemetinde artışa neden olmuştur. Eşmerkezli desen, %100 dolgu oranında sırasıyla 49,82 MPa ve 77,37 MPa olarak bulunan en yüksek çekme mukavemeti ve eğilme mukavemetini sergiledi. Bununla birlikte, en düşük çekme mukavemeti %20 dolguda 13,77 MPa ile Üçgen modelden, en düşük eğilme mukavemeti ise %20 dolguda 3B Bal Peteği modelinden elde edilmiştir. Sonuçlar, PETG filamentleri kullanılarak üretilen parçalar için baskı parametrelerinin dikkatlice seçilmesi gerektiğini gösterdi.

Anahtar Kelimeler: 3B Yazıcı, FDM, PETG, Doluluk Deseni, Doluluk Oranı.

‘’Dedicated to all who care about science, learning and investigate’’

ACKNOWLEDGEMENTS

I would like to thank my supervisor, Assoc. Prof. Dr. Ömer Yavuz BOZKURT for his knowledge, experience and valuable resources that devote their valuable time to me and support throughout the study. I am thankful for his encouragement and motivation. Your advice on both research and my career is invaluable.

I would like to thank Gaziantep University Mechanical Engineering Department for supporting my research in undergraduate and graduate studies since 2013 and providing me with all the opportunities.

I would also like to thank my instructor Dr. Özkan ÖZBEK, who supported me in all my thesis research and shed light on my path.

Finally, it was a great experience for me to complete my master's while working as an engineer. I am grateful to my mother Sevinç, my father İbrahim, my brother Semih Sefa and my fiancee Necmi, who always believed in me, supported me, and were always there for me.

This work is supported by Gaziantep University Scientific Research Center (BAP), through project under grant number MF.YLT.21.12.

TABLE OF CONTENTS

Page

LIST OF TABLES

Page

LIST OF FIGURES

Page

LIST OF SYMBOLS

°C	Degree Celsius
mm	Millimeter
MPa	Mega Pascal
Kg	Kilogram
G	Temperature
ΔL	Displacement
L0	Original Length
A0	Original Cross-Section
F	Maximum Load
σ	Engineering Stress
ε	Tensile Strain
L	Sample of Length
σ_f	Flexural Stress
ε_f	Flexural Strain
D	Maximum Deflection of Sample

LIST OF ABBREVIATIONS

PETG	Polyethylene Terephthalate Glycol
ABS	Acrylonitrile-Butadiene-Styrene
PLA	Polylactic Acid
FDM	Fused Deposition Modelling
SLS	Selective Laser Sintering
SLA	Stereolithography
AM	Additive Manufacturing
UTS	Ultimate Tensile Strength

CHAPTER I

INTRODUCTION

1.1 General Introduction

In today's world, the most important features that people, especially consumers, look for in a product that they need from the market are high quality, low cost, and high efficiency according to the application used. In this direction, suppliers try to meet consumer demands by the new development or production techniques in parallel to technological progressions by researchers. In this context, Additive Manufacturing techniques such as VAT Photopolymerisation, Material Jetting, Binder Jetting, Material Extrusion, Powder Bed Fusion, Sheet Lamination, Directed Energy Deposition, have been developed, in recent years, in order to produce the necessary products [1]. Some of these techniques with processing methods are seen in Table 1.1.

Table 1.1: Type of 3D Printing/Additive Manufacturing Technique

Processing Techniques	Classification of 3D printing
Vat photopolymerization	Stereolithography (SLA) Digital Light Processing (DLP) Continuous Digital Light Processing (CDLP)
Material extrusion	Fusion Deposition Modelling (FDM)
Material jetting	Material Jetting (MJ) Nanoparticle Jetting (NPJ Drop on Demand (DOD)
Powder bed fusion	Multi-Jet Fusion (MJF) Selective laser sintering (SLS) Direct Metal Laser Sintering (DMLS)/Selective Laser Melting (SLM) Electron Beam Melting (EBM)
Direct energy deposition	Laser Engineering Net Shape (LENS) Electron Beam Additive Manufacturing (EBAM)

The additive manufacturing (AM) methods satisfying the needs of the people who buy the product (customers) in a shorter time prevent the time consuming and measure the material reliability with low cost. Furthermore, it is a practical manufacturing method based on the principle of superimposing layers created according to the three-dimensional (3D) geometric data of objects using metal, plastic, composite and organic materials [2]. Additive manufacturing/3D Printing is spreading rapidly in both the industrial and domestic environment due to their many valuable properties (see Fig 1.1) [3].

The three-dimensional physical objects can be easily produced by the 3D printing technique with a simple visual view of the desired product [4]. The first commercialization of 3D Printing processes by Charles Hull was performed in 1980 [5]. Currently, the products by 3D printing/AM are used for many different fields, i.e., artificial production heart pump [6], jewelry collections [7], 3D-printed cornea [8], PGA rocket engine [9], steel bridge in Amsterdam [10], Also, its applications have a wide range from the aerospace industry as well as the food industry (see Fig. 1.2).

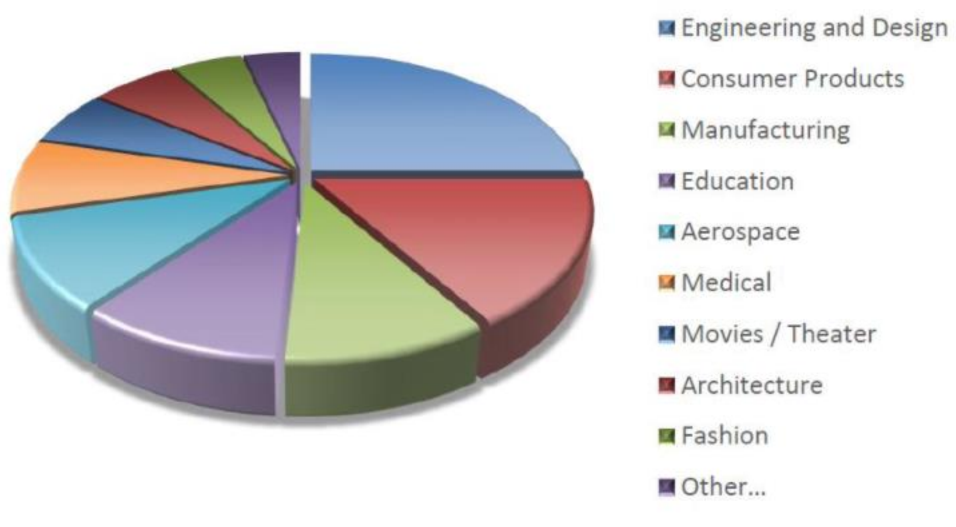

Figure 1.1 Industries where AM/3D Printing technology is spreading [11].

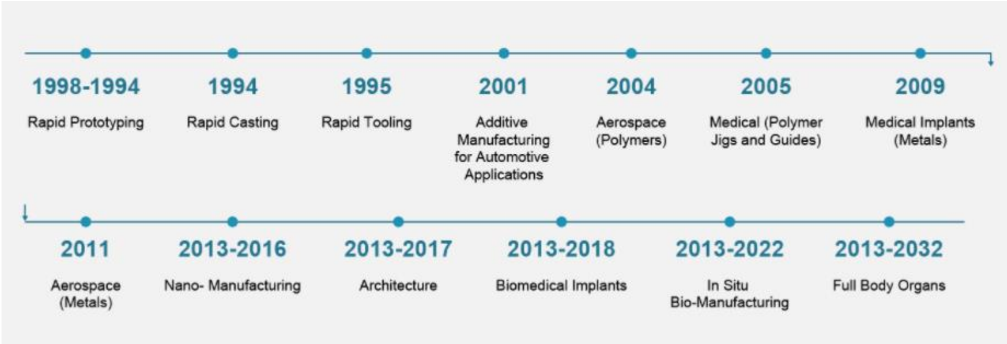

Figure 1.2 Additive Manufacturing/3D Printing application timeline [12].

The additive manufacturing technique or 3D Printing is widely used in specified industries, as it enables the production of small and complex parts at high quality and low cost [11]. The most common methods of additive manufacturing are Fused Deposition Modelling (FDM), Selective Laser Sintering (SLS), Stereolithography (SLA). Amongst them, FDM, which is based on the melting of thermoplastic filaments layer by layer to produce a product, is the most widely used material extrusion group of 3D printing techniques [1]. The technique was firstly used by S. Scott Crump who realized that molten polymer layer by layer creates three-dimensional parts to be used for the fabrication of a product in 1989 [13].

The advantages of FDM are as follows;

- *Ease of Accessibility*: Since the design consists of digital data, it can be easily transferred/shared.
- *Ease of Production:* Changes and corrections can be made quickly.
- *Customization:* The ability to easily produce personalized products.
- *Price-Performance:* Being efficient in terms of investment and production
- *One-Step Production:* The product price can be calculated before production.
- *Recycling Ease:* Using recyclable material.
- *Less Waste:* Minimum waste of material.

Although its various advantages, it has also some drawbacks. The limitations of three-dimensional printers for Fused Deposition Modelling are as follows;

- *Restricted Sizes:* It is difficult to produce large-size products at the moment.

- *Limited Materials:* Plastic and its derivatives are widely used in 3D printers. In addition, production can be made with some metals. However, sufficient diversity is not provided.
- *Waste Gases:* 3D printers can emit radiation and polymer materials that are harmful to human health.
- *Large Volume Production:* High energy is required to melt the materials used in 3D printers. Therefore, it is an element that increases the cost in multiple productions.

1.2 Research Objectives and Tasks

The main goal of this thesis is the investigation of the effect of printing parameters such as infill ratio, infill pattern on the mechanical behaviors of PETG filament is produced in a 3D printer.

The research tasks can be shown as follows:

I. An overview of the FDM technique in the 3D printer literature.
II. A detailed review of fused deposition modeling technique.
III. Determination of the parameters to be examined such as filament type, printing parameters, and mechanical experiments.
IV. Fabrication of samples with different parameters using PETG filament by 3D printer.
V. Performing of uniaxial tensile and three-point bending experiments
VI. Discussions on findings obtained from each experiment according to parameters,
VII. Assessment of conclusions obtained from the above tests, respectively.
VIII. Summarization of the effect of infill ratio and infill pattern on the considered mechanical responses of samples.

1.3 Layout of Thesis

A brief literature survey about 3D Printer technology is presented in Chapter 2. The material used in studies, and methods including fabrication methods and mechanical experiments (tensile, three-point bending) is given in Chapter 3. Chapter 4 presents the findings and discussions according to experimental results. Conclusions are revealed in Chapter 5.

CHAPTER II

LITERATURE SURVEY

2.1 Introduction

A basic literature examination related to thesis studies is presented in this chapter. Firstly, the types of Additive Manufacturing/3D Printing methods are summarized and some studies are given to provide knowledge about them. Then, the literature studies interested in the materials fabricated by the 3D Printing method are given. Lastly, the parameters used in 3D Printers are shown with scientific works.

2.2 Literature Survey on Basic Type of 3D Printer Production

The researchers, who aims to make life easier for people, are always looking for new materials having low cost, low volumes, small components, environmentally friendly. Today they are focused on additive manufacturing or 3D Printing technology due to its outstanding properties such as easy fabrication of complex-shaped products, cheaper than traditional manufacturing methods. Nowadays, 3D Printed products are used in various areas such as automotive, medical, automobile, and space.

Ngo et al. [2] and Bikas et al. [14], pointed that additive manufacturing was a new method with a wide range of materials, including plastics, metals, and ceramics, relatively to traditional methods, and is becoming increasingly common. Due to the widespread use of additive manufacturing, research on additive manufacturing has increased tremendously. Researchers have performed various studies to improve both process and part quality.

There are many different production methods for the additive manufacturing type. In this thesis, three of the most common ones are mentioned. These are Fused Deposition Modeling (FDM), Selective Laser Sintering (SLS), Stereolithography (SLA). The following sections are presented for basic knowledge and short literature for these techniques.

2.2.1 Fused Deposition Modeling (FDM)

FDM's working principle is as follows: forced a polymer filament (ABS, PLA, PETG, STH, etc.) to pass from a hot nozzle in order to molten and then placed molten material on a building platform according to the desired geometry by moving on three axes. It provides a layer-by-layer production. By the way depending on the geometry of the products, the filament materials can be classified as built material and support material. The first one is used to form product itself. On the other hand, second one is employed for the construction of auxiliary geometries (supports) to help the production of complex or thin geometries that requires support. After the production of the prototype, all support materials are removed carefully from the product. The design and material of support can also affect the products' mechanical or physical properties. Not only the supports, but also the several parameters of 3D printing process such as nozzle structure, filament feeding system, building platform, filament material, print speed, print temperature, etc. can have influence on the final properties of the products. There are several scientific studies that dealt with the filament materials used in the FDM technique.

Hsien et al. [15] expressed that the most preferred and accepted model was FDM in terms of flexibility, higher printing speed, low cost, high strength, and toughness. They defined it as a method of depositing thermoplastic filament materials (e.g. ABS, PLA, PC, PS, Nylon, and PET) layer-by-layer to create 3D parts using heat from a semi-solid during extrusion to remove them from a nozzle.

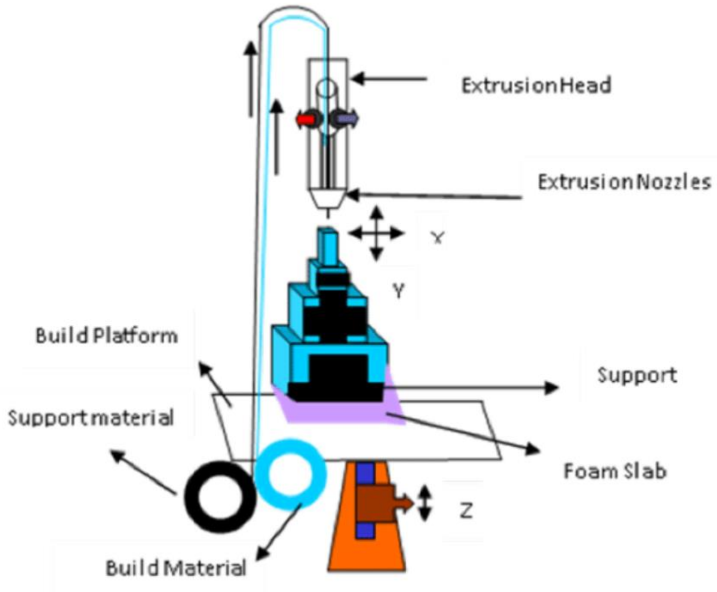

Figure 2.1 FDM Material Extrusion [16]

Many FDM process parameters play an important role in the performances of the produced materials. Ahn et al. [17] and Bagsik et al.[18] mentioned that the common process parameters used for prototypes to be produced in FDM can be given as print speed, layer height, raster angle, fill gap and build temperature. All these process parameters affect mechanical properties, surface finish quality, printing time, and filament consumption. Some of these are given in Figure 2.2.

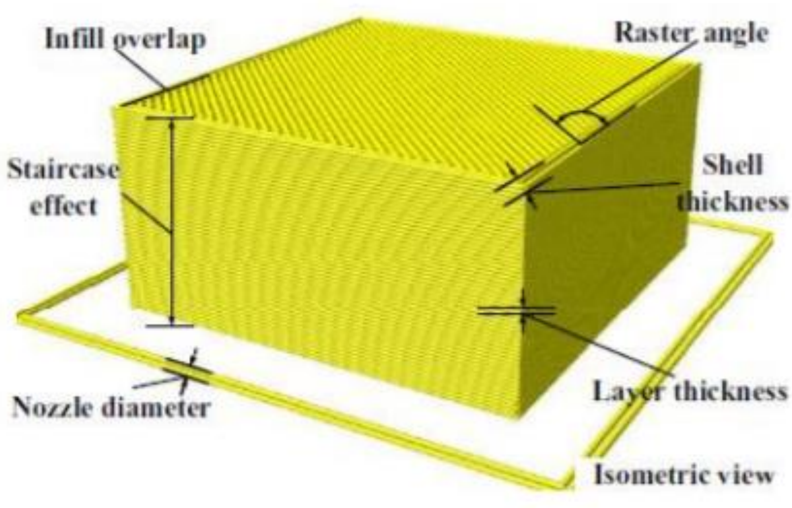

Figure 2.2 FDM process parameters [16]

In standard production techniques such as extrusion or injection molding, hardness and strength increase as a result of the reinforcement process of natural fibers with plastics. Mazzanti et al. [3] investigated whether this process also applies to components produced with FDM. As a result, he saw that the mechanical properties of acrylonitrile-butadiene-styrene (ABS) and PLA did not benefit from bio-fillers. In addition, it has been seen that polymers such as Polyolefins (PE, PP based) have higher performance.

Mazzanti et al. [3] investigated the effect of natural polymers on the mechanical properties and filament cost produced by the FDM 3D Printing Technique. They found that natural fibers had a mild reinforcing function, improving stiffness and strength and decrease of the fiber cost. In addition, natural fibers did not alter biodegradability in the final material.

Ahn et al. [17], investigated the properties of anisotropic materials produced by the fused deposition modeling technique. They found that the tensile strength affected by the air gap and raster orientation. Bagsik et al. [18], were also investigated the mechanical properties of the products fabricated with fused deposition modeling. It was notified that build direction influences the mechanical properties.

Anakhu et al. [19], investigated the problems of traditional pattern making and the challenging of FDM-printed patterns for sand casting and suggested solutions. The advantages of FDM-printed pattern for sand casting was reported as optimized layer height, surface finish quality, reduced cohesiveness.

Cailleaux et al. [20] studied the production of pharmaceutical solid oral forms of drugs for use in the treatment of rare diseases and certain populations that require special doses or release kinetics, using heat-sensitive components with the Fused Deposition Modeling (FDM) production technique.

Li et al. [21] investigated the potential to fabricate prototypes with locally-controlled properties by changing deposition density and deposition orientation, the fabrication process, and the mechanical properties in FDM technology. They suggested equations to find the elastic constants of FDM samples

Suárez et al. [22] studied significant environmental impacts, energy used, materials used, and waste generated by these technologies in FDM technology. They established a method for applying eco-design principles taking into account the specific features of additive manufacturing.

Melocchi et al. [23] designed a conceptual map to move through the evolution of the design of the printed dosage forms/drug delivery systems for usage in pharmaceutics. Manufactured by FDM no drug products had been approved yet because of quality assurance and quality control topics. In addition, all those studies could help to develop ideas and studies will light for the future in the sector of pharmaceuticals.

Haghsefat et al. [24] showed that ABS and PLA materials are widely used as consumables for FDM 3D (Additive Manufacturing) printers. They noticed differences in the performance of these two materials. Problems such as local bending, cracks in between, broken wires, clogged nozzles, odors, and wire drawing were encountered in the printed samples. They argued that the hardness should be increased in order to increase the efficiency of ABS and PLA materials.

Wagari et al. [25] investigated the effects of FDM process parameters using ULTEM 9085 material, which is a type of thermoplastic material. Five process parameters such as air gap, raster width, raster angle, number of contours, and contour width were considered in their investigation. The lowest and highest tensile strength values of these parameters were recorded as 30 MPa and 87 MPa, respectively. They found that the parameter most affecting the shrinkage property is raster angle.

2.2.2 Selective Laser Sintering (SLS)

SLS is an additive manufacturing technique, which is shown in Figure 2.3, and the laser-based is used as the source and powder material is used for the production of parts. The working principle is as follows: There is a table in which the model will be produced in a construction pool filled with powder material. By moving the table up and down, the volume where the layer will be created is provided. When the table comes down, a laser beam is sent to the powder material remaining on the table. After this melting and then solidifying layer is completed, the platform goes down. With the help of a roller (roller), the powder is laid on the first layer on the platform and the beam from the laser source solidifies the new layer and connects it to the previous layer. This process, which is mentioned by sintering, can be applied not only to plastic but also to materials such as aluminum, stainless steel, titanium, nickel alloy, cobalt chrome, ceramic, and polyamide.

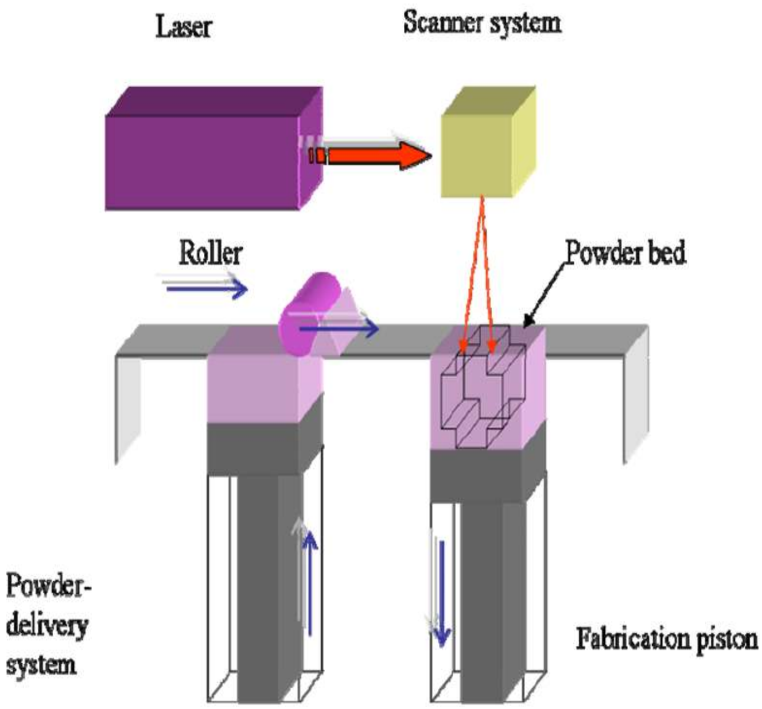

Figure 2.3 Scheme of Selective Laser Sintering (SLS) Technique[24]

Peltola et al. [26] successfully used to construct prototypes of minipig's mandibular condyle scaffolds using the SLS fabrication technique. Due to SLS tech, these scaffolds replicated the desired anatomy well within three hours.

Kumar [27] studied the SLS method on polymers and nylon to create prototypes for audio-visual aid and form-fitness testing. He notified the SLS method as a reliable for rapid prototyping and an emerging technique for rapid manufacturing.

Jain et al. [28] conducted research on the latency problem in the production of SLS prototypes. With this study, he solved this problem by developing an algorithm during optimum part construction to improve tensile strength.

2.2.3 Stereolithography (SLA)

SLA technology is based on resin hardening, which normally is liquid at room temperature, with the point ultraviolet laser beam. The first layer occurs with the resin layer adheres and the hardening process continues until producing the layer. After the layers are complete, the sample took from the resin pool. The last step is to separate support from the sample.

SLA is one of the most reliable and precise 3D printing methods, prototyping, and high-resolution industry-grade applications. The feature that distinguishes it from other additive manufacturing techniques is that the layer thickness of stereolithography is much less (0.05 to 0.10 mm) [29]. In addition, it is possible with this method to create larger pieces up to two meters in length with small pieces of high resolution as seen in Figure 2.4.

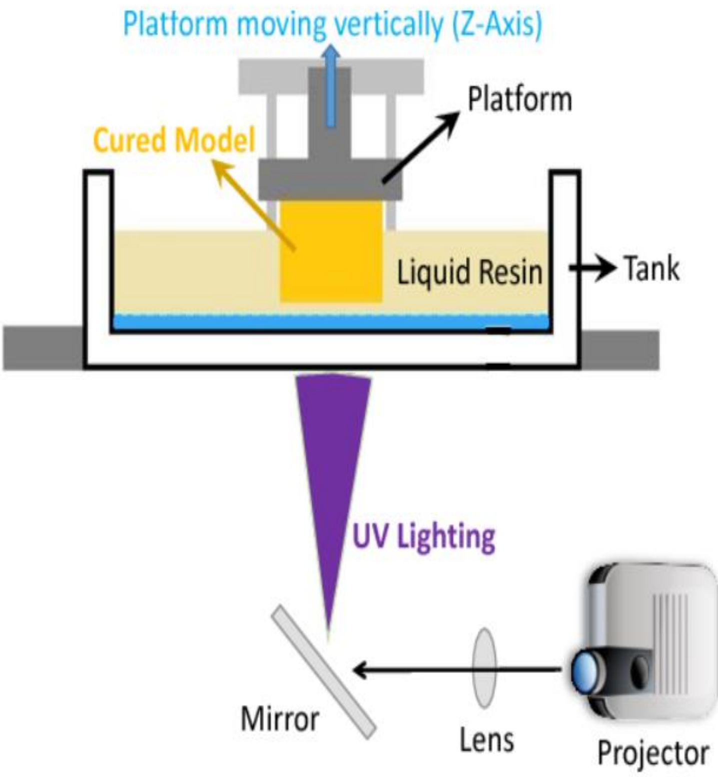

Figure 2.4 Schematic representation of the Stereolithography (SLA) System [29]

Yang et al. [30] observed that the surface quality of SLA parts is difficult in precision parts due to the ladder steps caused by the additive manufacturing process. In his article, he made this possible by ultra-high pressure atomized coating with polyethylene wax emulsion, using the optimum coating parameter to improve precision manufacturing without damaging SLA parts.

Hata et al. [31] investigated the production of material (PMMA - polymethyl methacrylate), which is widely used in dentistry, by stereolithography (SLA) additive manufacturing technique. SLA evaluated the printability and viscosity, mechanical properties, shear bond strength, degree of transformation, physicochemical properties of a new PMMA-based resin for 3D printing. As a result, PMMA material used for the first time has been a potential candidate for dental applications.

Kara et al. [32] fabricated the microfluidic chips used in nanomedicine by stereolithography (SLA), as fabrication is very difficult due to the complex geometry of the channels. Thus, they succeeded in shortening the nanomedicine development process while maintaining high-quality standards, allowing for customization of the design process for the serial production of nanomedicine, and enabling easy scale-up.

Grzeszczak et al. [33] investigated the suitability of stereolithography (SLA) to produce synthetic trabecular bone and evaluated its mechanical properties by compression and screw tensile tests. Cadaveric specimens in SLA-imprinted poly (lactic acid) had higher tensile strength than existing synthetic models and models produced with FDM.

Montal et al. [34] studied how the materials printed by stereolithography (SLA) behave under different stress states and strain rate regimes and analyze the effects of parameters such as cure time, temperature, compression angles, printing resolution. For this purpose, tensile and compression tests were carried out at different strain rates. They found the effects of these parameters on SLA prototypes.

2.2.4 Comparison of 3D Printing Techniques

FDM, SLS, and SLA are seen as the most common Additive Manufacturing techniques in scientific studies. The comparison of these techniques is summarized in Table 2.1. Additionally, some prototypes produced by them are given in Figure 2.5.

Table 2.1 Comparison of 3D printing techniques [14]

Method	Working Progress	Material Used	Pre-Process	Resolution	Strength	Roughness
FDM	the build platform layer by layer	ABS PLA PETG	Layer Support Creation	Medium	Good	Medium
SLS	Sintering of powder with CO2 laser	Polyamide, Polystyrene, Carbon fiber Aluminum added polyamide Stainless.	-	Weakness	Good	Weakness
SLA	Photopolymer material solidification with UV light	Resin based materials acrylic epoxy	Layer Support Creation	Good	Medium	Good

(a) FDM (b) SLS (c) SLA

Figure 2.5 Some prototypes of additive manufacturing techniques [35]

There are various studies devoted to the comparison of AM techniques in the literature. Some of them are given as follows;

Terekhine et al. [36] investigated the quasi-static and fatigue loading on the polyamide 12 (PA12) specimens manufactured by FDM, SLS, and Injection Molding (IM). The obtained results from FDM and SLS were compared to the IM technique in terms of flexural and fatigue response of the samples. The samples fabricated by FDM and SLS showed better fatigue characteristics than the samples produced by IM.

The biggest problem of 3D printing technology, which has been developing rapidly for 40 years, is cracking in ceramic materials. Jia-wei Cai et al. [37], have been able to produce high-complex shaped quality ceramics by avoiding the internal stress caused by rapid cooling in major manufacturing techniques including binder sputtering (BJ), stereolithography (SLA) and fused deposition modeling (FDM).

Sun et al. [38] produced the polymeric cage prototype using FDM and SLS methods and investigated static and dynamic crushing. In the experimental results, it was seen that the cages produced with SLS exhibited good energy absorption performance under quasi-static compression, but were affected by the impact. The cages produced with FDM provided good energy absorption under both quasi-static and dynamic compression.

Kafle et al. [39] presented a comparison by correlating polymer material-process properties with three different 3D printing techniques, FDM, SLS, and SLA. They investigated using a highly innovative 4D printing prototype used in robotics and biomedical fields recently. The meaning of 4D printing is that the materials produced with a 3D printer can be shaped in 4 dimensions after production by using different printing techniques during production. After being produced, FDM and SLA can be processed better than SLS due to their easy manufacturing processes and compatibility. They advanced that it will also be a guide for 3D/4D printers in terms of applicability.

Choudhari et al. [40] Selective Laser Sintering (SLS), Stereo-lithography (SLA), and Fused Deposition Modeling (FDM) techniques, which are 3D manufacturing technologies, have investigated the cost and surface quality stages for an optimum design. They found that for smooth surface, uncomplicated parts, the best surface quality was the FDM technique in terms of minimum production cost and minimum construction time (10 min). For the SLA method, the material cost was high and the printing speed is medium (13 min) in the second place. The SLA method, on the other hand, was considered mechanically complex and ranked third for print length (17 min).

2.3 Literature Survey on 3D Printer Materials Used in FDM Technique

PLA, ABS, and PETG materials called pure polymers are widely used in 3D printers and have been frequently studied in scientific studies. PLA is printed at lower temperatures than ABS. Since PLA is completely natural, it has a biodegradable structure and with this feature, it is much more environmentally friendly than many filament types. Since PLA is not a harmful substance to health, it can be used in products that can come into contact with the human body, and because they have a shiny structure, they are generally preferred in luminous products. PLA has low moisture resistance and cannot be easily bonded. It is very easy to print compared to ABS, but the technical feature of ABS is superior. ABS is known for not emitting high emissions and bad odors during printing. PETG is the most widely used plastic type in the world because it is easier to use than PLA and more durable than ABS. It is as easy to manufacture as PLA and fully recyclable as a raw material. PETG filament does not have any identified disadvantages.

Figure 2.6 Mechanical properties of materials [35]

Zharylkassyn et al. [41] produced the FDM technique samples using ABS, PLA, Nylon, and other resins to investigate the effect of process parameters of different materials. They prepared these samples based on the production parameters in the 31 articles they reviewed in total. They observed that ASA and Nylon parts with low layer thickness were less durable than ABS and PLA.

Hsien et al. [15] presented that PLA and PETG filaments provided better tensile and compressive stress than other materials. They observed that the mechanical properties of parts produced with PLA and PETG filaments increased as the printing temperature increased. On the other hand, with the increase of the printing speed the mechanical properties of products with PLA filaments were increased but PETG ones decreased. They found that the mechanical properties of PLA were greater than those of PETG, excluding Young's modulus and strength.

Leite et al. [42] investigated the water absorption and tensile characteristics of parts produced using PLA filament in FDM technique. They found the best tensile behavior values with 60% infill ratio, 220ºC extrusion temperature, 0º/90º raster angle, and 0.1 mm layer thickness. It was measured as the worst water absorption behavior for PLA with an extrusion temperature of 200ºC and a layer thickness of 0.2 mm.

Mirornet al. [43] produced samples from Polylactic acid (PLA), Polycarbonate (PC), Polypropylene (PP), and Polyamide 12 (PA12) using the FDM technique. Samples were subjected to the Charpy test and analyzed. While the PLA material was cracked at room temperature without the notch, the other materials were notched and additionally cooled the PP and PA12 materials down to -40°C. They found that PA12 material is the most suitable material in areas where impact strength and low temperature were important.

Doshi et al. [44] studied the direct effect of printing parameters on mechanical properties such as tensile strength, stress, Young's modulus for ABS and PLA materials in FDM technique. They showed that the parameters of layer thickness, infill ratio and pattern, printing speed, structure orientation, and raster angle are the most important parameters that directly affect the mechanical properties.

Chawlaa et al. [45] searched the flexural strength of specimens printed with composite filaments which were prepared in-house with secondary recycled ABS 90% by weight reinforced with an equal percentage of bakelite powder, Fe powder, and wood dust. The study was commonly focused on the effect of three printing parameters (raster angle, infill ratio, and infill speed) of FDM technique. They informed maximum peak strength (flexural) for 0° raster angle, 20 mm/s printing speed, and 80% infill ratio.

Ćwikła et al. [46] produced low-cost PLA and ABS materials with parameters such as infill pattern, direction, shell thickness, and printing temperature. They found that it was not always observed that the strength and hardness of the specimen increased as the thickness of the shell increased in the cross-section.

2.4 Literature Survey on 3D Printer FDM Production Parameter

There are several process parameters of the FDM technique such as infill ratio, infill pattern, nozzle temperature, table temperature, feeding speed, layer thickness and orientation, raster angle, and nozzle diameter according to 3D printer machines types. These process parameters have remarkable effects on the mechanical characteristics of the printed materials. The following parts have presented the studies related to the investigation of FDM process parameters.

Domingo et al. [47] performed the Finite element analysis (FEA) simulations to simulate the parts they produced using the FDM method with polycarbonate (PC) material. They measured the mechanical response of the materials during bending and torsion physical tests.

Chamil et al. [48] observed that the harmony of the printing speed and melting temperature of the filament is very effective in preventing melting. Polymers were poor thermal conductors, observed that speeds above 90 mm/s melt the filament and thus poor adhesion between neighboring layers and particles, resulting in a lower strength. In the experimental trial, only the printing speed changed and other parameters (such as the set nozzle temperature) remained constant. They found that the optimum printing temperature for PLA filament was 215 °C. In addition, when the infill ratio increased, the porosity decreased and the mechanical bond between the layers increased. They tried seven different infill patterns and chooses the linear model that had the lowest porous structure, which was due to its good adhesion in terms of interlayer bonding.

Dezaki et al. [49], investigated the effects of different patterns and infill ratios on the surface roughness and tensile properties of the materials produced by FDM technique.

The Concentric and Grid patterns showed the highest strength values. They observed that 10% and 40% infill ratio were almost the same mechanical properties for the Triangular pattern sample. The weakest sample was the Zigzag pattern for %30 and %50 infill ratio because of messy design and poor adhesion.

Pandzic et al. [50] stated that the "Concentric" infill patrern gives the highest tensile strength and yield strength compared to other models, and reported that when reduced from 100% filling to 90%, the tensile strength is only 15%, yield strength 20% and the printing time was reduced by 30%.

Leite et al. [42] investigated the effect of temperature on the mechanical characteristics of PLA materials. It was found that when the temperature increased, the adhesion between the layers increased and tended to become more brittle.

Kariz et al. [58], using the FDM technique, examined the mechanical properties of the samples produced with PLA filament with 0%-50% weight wood content. They found that the tensile strength of the 10% wood reinforced sample increased from 55 MPa to 57 MPa. It was observed that 50% wood content filaments decreased to 30 MPa so weakened 25 MPa strength. They have seen that as the wood content increased, the surface roughness increased, the gaps increased and the printer nozzle was clogged.

2.5 Conclusion on Literature Survey

So far, most of the scientific work devoted to the investigations of the effects of production parameters for PLA and ABS materials which are the most common materials in 3D printing. Although a limited number of studies are seen for PETG filaments, no detailed systematic work has been reported on the effects of process parameters on the mechanical responses of the PETG materials manufactured by 3D Printing. Thus, this thesis describes an experimental study on the effect of 3D Printing production parameters such as infill ratio and infill pattern for PETG filaments subjected to tensile and three-point bending loadings.

CHAPTER III

MATERIALS AND METHOD

3.1 Materials

The filament used in this study, as seen in Figure 3.1, is the PETG (Polyethylene terephthalate glycol) procured from Porima Polymer Technologies Inc., Turkey.

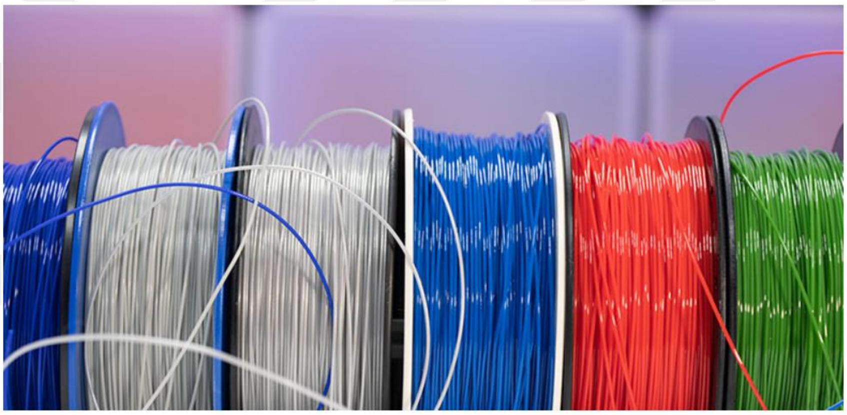

Figure 3.1 PETG (Polyethylene Terephthalate Glycol) filaments [51]

British scientists John Whinfield and James Dickson used a process called esterification by heating Glycols with terephthalic acid to create polyethylene terephthalate (PET) in 1941 [52], which is known as the first PETG usage. Some features of PETG filaments are given below.

- Used for water bottles, food packaging, and countless other plastic products, as seen in Figure 3.2.
- High hardness, durable, resistant to impacts, and lightweight.
- The printing temperature is usually between 220°C–250°C.
- Lifting and cracking problems are rarely encountered during cooling.
- More flexible and odorless than ABS and PLA.
- Rigidity and mechanical properties are better than ABS.

- Compared to PLA, it is easy to manufacture and can run at up to 20% higher print speeds [53].

Figure 3.2 PETG usage in; (a) Plastic bottles (b) Textile (c) Dental aligners (d) Packaging industry (e) Medical packaging [54]

3.2 Sample Fabrication by Fused Deposition Modeling

In order to fabricate a product with Fused Deposition Modeling production technique, first of all, a geometry should be digitally developed and a G-code which has information about the printing parameters must be generated for this geometry using a slicer software. Then, production is carried out with the selected filament. The last step is the cleaning of the support parts if it's there. The production flow is given in Figure 3.3.

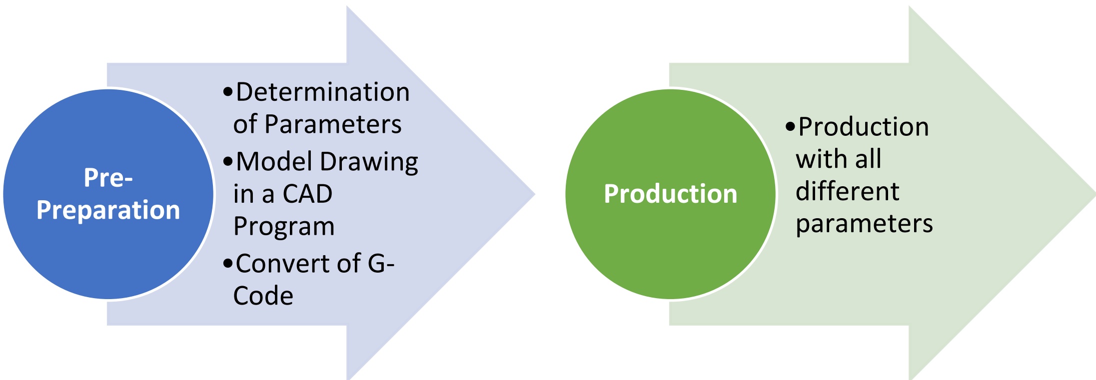

Figure 3.3 Fabrication steps

- *Determination of Parameters:*

The process parameters used in the experimental study are given in Table 3.1 and when the production of samples, these parameters are always constant.

Table 3.1 Constant process parameters

Constant Process Parameters	**Value**
Layer thickness (mm)	0.25
Table temperature (°C)	80-90
Environment temperature (°C)	25
Number of lower shell layer	4
Number of upper shell layer	4
Number of outer walls	>2
Print speed (mm/s)	40-110

Model Drawing in a CAD Program

The product model to be produced is drawn in CAD programs beforehand and saved in STL format. The file with STL extension is uploaded to 3D Printer to form materials with desired geometry as seen in Figure 3.4.

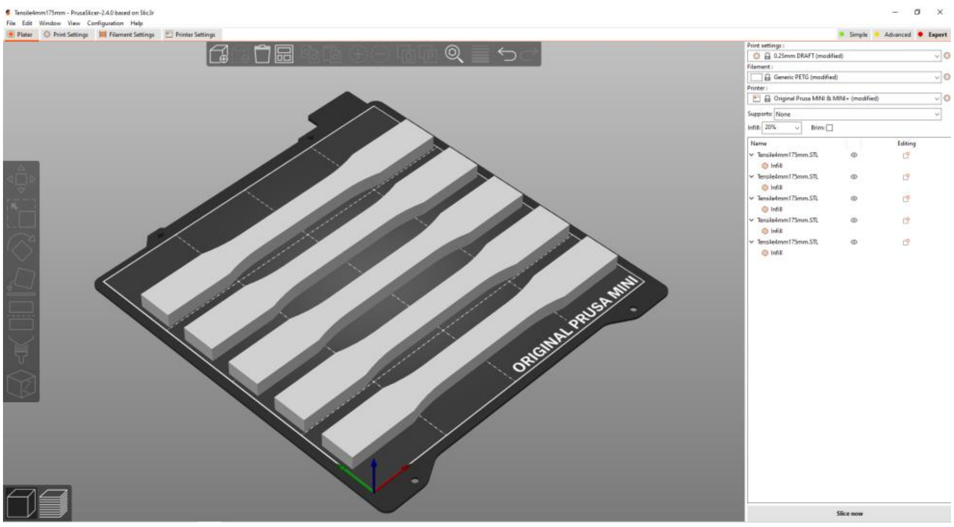

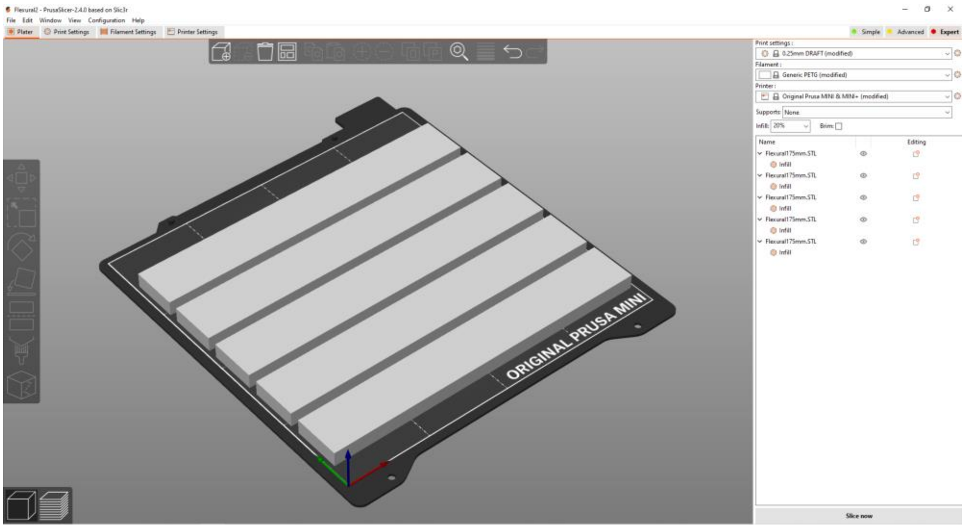

Figure 3.4 The samples on Prusa Mini

<u>Convert of G-Code</u>

One of the three-dimensional object slicing programs is PrusaSlicer, and the interface of the PrusaSlicer program is shown in Figure 3.5.

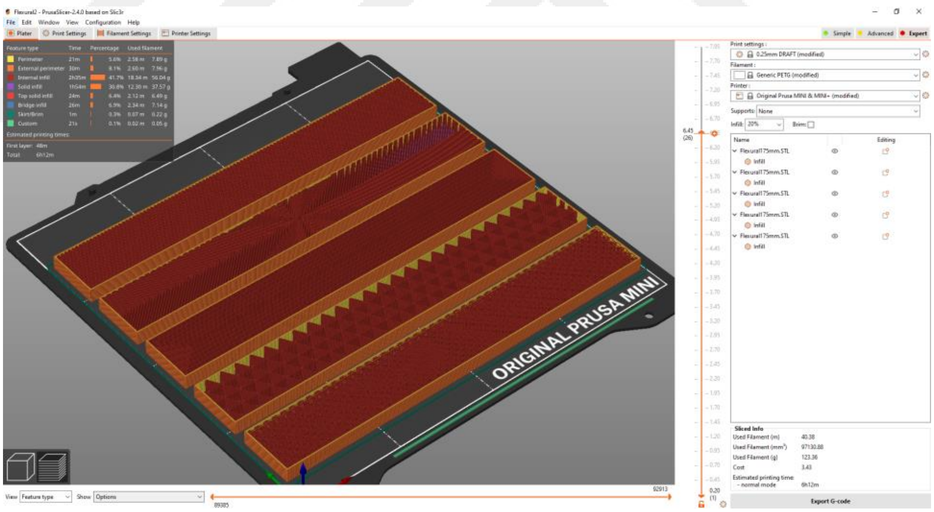

Figure 3.5 PrusaSlicer

<u>Production with all different parameters</u>

Then the model is imported into the PrusaSlicer program, the specified parameters are entered and G-Code is generated.

Finally, the PETG filament passes through the hot extruder and melts through a thin nozzle, and falls onto the platform in the form of a string structure. While this process is being done, it is controlled by the computer with the help of G-Codes. Thanks to this program, production takes place in the desired dimensions, with the desired variable and fixed parameters. According to the coordinates in the G-Code, each rope cools and solidifies by overlapping layer by layer and forms a rigid bond with the layer below. The Original Prusa Mini 3D Printer was used for all fabrications as seen in Figure 3.6.

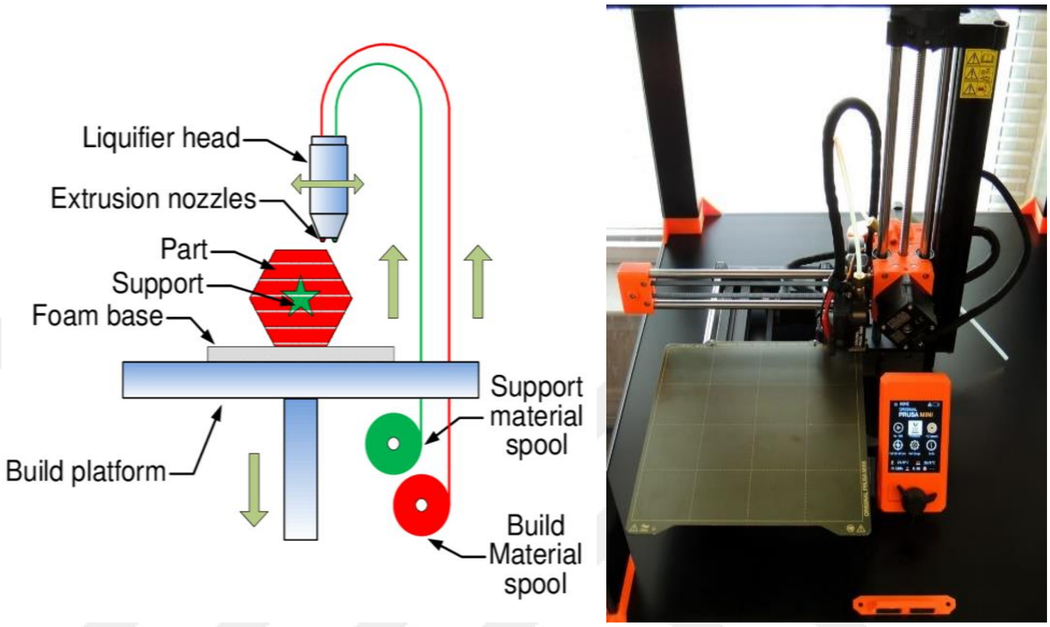

Figure 3.6 FDM Schematic showing (a) Basic components [55], (b) Original Prusa Mını

The process parameters which are seen in Table 3.2 were kept constant during fabrication. In this study, the effects of infill ratio and infill pattern were only examined.

Table 3.2 Properties of Original Prusa Mini

Constant Process Parameters	**Value**
Volume (cm^3)	18
Max. Print Speed (mm/s)	200+
Layer Height (mm)	0.05-0.25
Max. Nozzle Temperature (^oC)	280
Max. Table Temperature (^oC)	100
Size (cm)	38*33*38
Weight (kg)	4.5

Using these process parameters, five samples were printed for each configuration. During the production, variable parameters such as infill pattern and infill ratio stated below were taken as the basis. The sample weight and thickness information were given in Table 3.3.

Table 3.3 Weight and thickness informations of samples

Naming	Infill Ratio (%)	Weight for Tensile Test (g)	Weight for Flexural Test (g)	Thickness (mm)
Archimedes	20	12.87 ± 0.35	17.57 ± 0.02	7.86 ± 0.10
	40	16.53 ± 0.06	23.39 ± 0.17	7.87 ± 0.07
	60	19.56 ± 0.09	28.70 ± 0.15	7.85 ± 0.09
	80	22.76 ± 0.65	34.66 ± 0.60	7.87 ± 0.10
	100	26.48 ± 0.13	39.37 ± 0.07	7.90 ± 0.00
3D Honeycomb	20	12.93 ± 0.20	15.64 ± 0.08	7.90 ± 0.08
	40	16.98 ± 0.02	24.74 ± 0.39	7.90 ± 0.06
	60	21.06 ± 0.31	31.58 ± 0.43	7.94 ± 0.06
	80	24.93 ± 0.39	38.23 ± 0.14	7.92 ± 0.11
Octogram	20	12.87 ± 0.17	17.31 ± 0.07	7.95 ± 0.08
	40	16.35 ± 0.20	24.04 ± 0.45	7.96 ± 0.10
	60	19.34 ± 0.26	29.04 ± 0.42	7.93 ± 0.14
	80	22.82 ± 0.28	34.94 ± 0.65	7.97 ± 0.07
	100	26.15 ± 0.36	40.66 ± 0.16	7.93 ± 0.08
Gyroid	20	12.83 ± 0.00	15.51 ± 0.08	7.92 ± 0.04
	40	16.44 ± 0.03	24.30 ± 0.13	8.00 ± 0.06
	60	19.67 ± 0.03	29.08 ± 0.43	7.94 ± 0.02
	80	23.22 ± 0.07	34.45 ± 0.48	7.93 ± 0.05
Triangle	20	12.45 ± 0.24	17.11 ± 0.02	8.00 ± 0.04
	40	15.68 ± 0.28	23.73 ± 0.70	8.05 ± 0.03
	60	19.47 ± 0.32	28.93 ± 0.21	8.05 ± 0.07
	80	22.70 ± 0.36	35.10 ± 0.11	8.01 ± 0.08
Rectilinear	20	12.59 ± 0.17	17.60 ± 0.04	7.85 ± 0.07
	40	16.07 ± 0.24	23.49 ± 0.26	7.87 ± 0.05
	60	19.45 ± 0.28	28.85 ± 0.00	7.87 ± 0.06
	80	23.02 ± 0.37	35.47 ± 0.17	7.83 ± 0.09
	100	26.12 ± 0.20	40.56 ± 0.33	7.86 ± 0.04

Table 3.3 (cont.)

Honeycomb	20	13.65 ± 0.27	18.94 ± 0.02	7.95 ± 0.12
	40	17.82 ± 0.31	25.77 ± 0.00	7.95 ± 0.15
	60	21.03 ± 0.39	31.93 ± 0.62	7.98 ± 0.11
	80	24.06 ± 0.45	36.84 ± 0.67	7.97 ± 0.06
Concentric	20	12.78 ± 0.21	18.56 ± 0.01	7.93 ± 0.08
	40	16.20 ± 0.25	23.98 ± 0.43	7.98 ± 0.09
	60	19.67 ± 0.33	29.57 ± 0.51	7.95 ± 0.08
	80	22.75 ± 0.36	35.21 ± 0.01	7.91 ± 0.06
	100	26.14 ± 0.38	40.48 ± 0.77	7.85 ± 0.05

3.3 Mechanical Characterization

All samples were tested by two different test methods to examine the effects of different process parameters on the mechanical behaviors of products printed using PETG filaments. Firstly, tensile test according to ASTM D638 standard [56], and secondly, three-point bending test according to ASTM D790 standard [57] were conducted. While performing all these tests, the Shimadzu AG-X Series universal testing machine device in the Gaziantep University Mechanical Engineering Mechanics Laboratory was used.

3.3.1 Uniaxial Tensile Test

The sample to be tested in accordance with the ASTM D638 [56] Standard is placed in the machine, and a tensile force is applied until it breaks. During the application time of the force, the amount of elongation in the standard section is recorded reciprocally with the applied force.

The tensile strain, ε, and engineering stress, σ, are evaluated using elongation and force data according to equation 1 and 2, respectively.

$$\varepsilon = \frac{\Delta L}{L_o} \tag{1}$$

$$\sigma = \frac{F}{A_o} \tag{2}$$

where ΔL, L_o, A_o and F are the elongation, original length, original cross-section area and maximum load, respectively.

The sample geometry used in uniaxial tensile experiments is given in Figure 3.7 the crosshead speed of 5 mm/min was used for loading rate in tensile experiments as seen in Figure 3.8. Five samples were tested to ensure experimental reliability and their averages were used in the results.

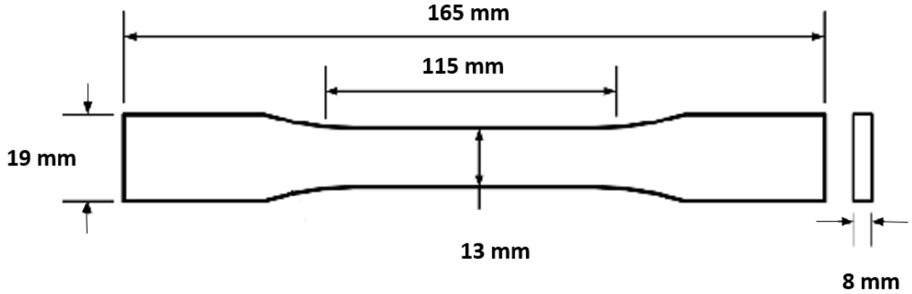

Figure 3.7 Sample geometry for tensile test of FDM printed parts [56]

Figure 3.8 Tensile testing

3.3.2 Three-Point Bending Test

In order to evaluate the effects of process parameters on the flexural behaviors of parts produced using PETG filaments, the samples printed in the dimensions shown in

Figure 3.9 were loaded in the transverse direction according to ASTM D790 [57]. The sample was placed by centering on two support points as shown in Figure 3.10. Span length which is 16 times of thickness were used as 128 mm. The force was applied to the center of sample. Thus, compressive stresses were created on the upper side of the sample and tensile stresses on the lower side.

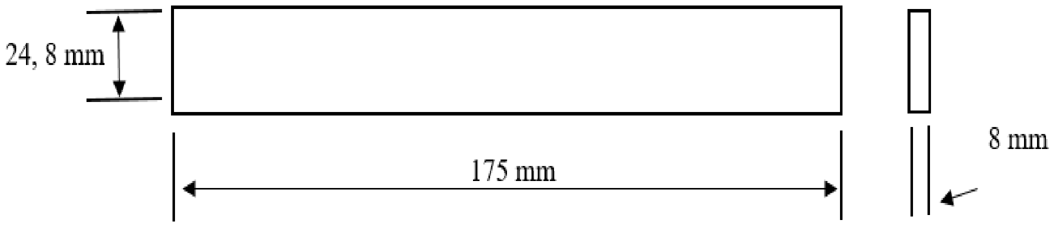

Figure 3.9 Three-point bending test sample for FDM [57]

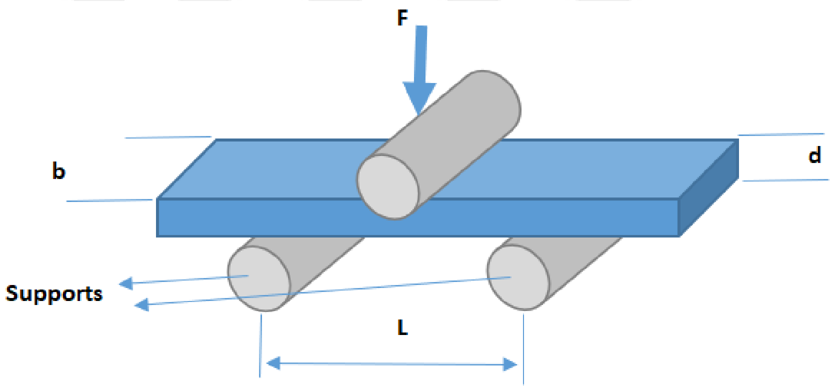

Figure 3.10 Three-point bending test method for FDM

The test sample was loaded at a speed of 3.41 mm/min, as seen in Figure 3.11. At least, five numbers of tests samples were used for each configuration. The flexural stress (σ_f) and flexural strain (ε_f) of the samples were calculated by the following equations:

$$\sigma_f = \frac{3FL}{2bd^2} \quad (3)$$

$$\varepsilon_f = \frac{6Dd}{L^2} \quad (4)$$

where F and D are the maximum flexural load and maximum deflectons of the sample, respectively. Also L, b and d represent the span length, width and thickness of the samples, respectively.

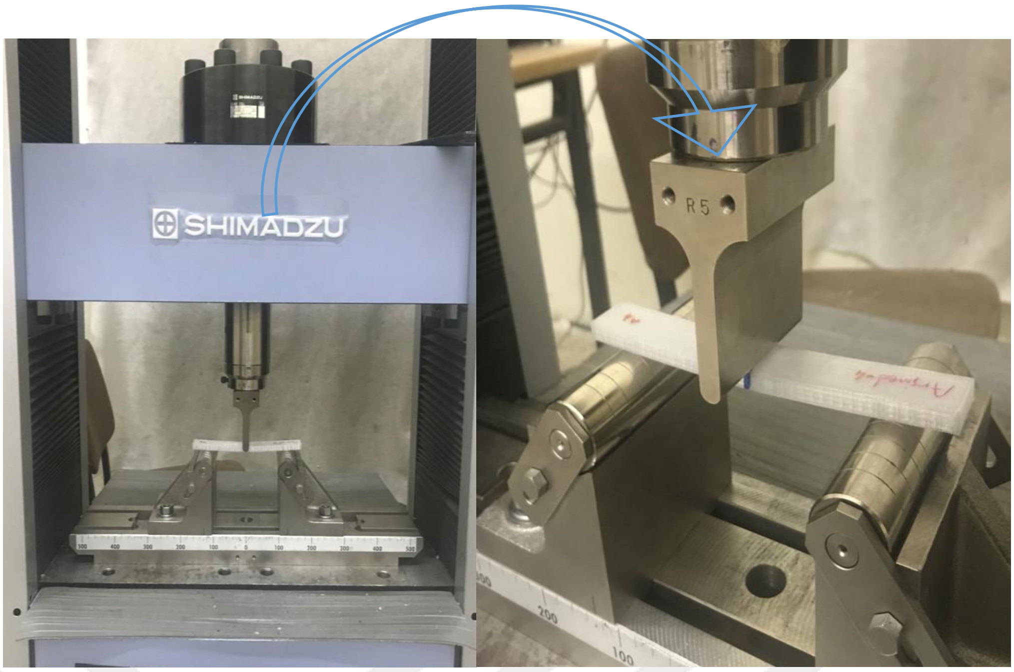

Figure 3.11 Three-point bending test

CHAPTER IV

RESULTS AND DISCUSSIONS

In this section, the results of tensile and three-point bending tests are presented that the most basic researches to determine the fundamental mechanical properties of PETG filament. In order to investigate the effect of infill ratios, which is one of the parameters previously mentioned in the literature section, on mechanical properties, 20%, 40%, 60%, 80%, and 100% infill ratio were studied, respectively. These samples have been produced using eight different (Archimedes, 3D Honeycomb, Octogram, Gyroid, Triangle, Rectilinear, Honeycomb, Concentric) infill pattern, as seen in Fıgure 4.1. Five numbers of the test sample for each configuration have been used to ensure experimental reliability and the average of them has been used in the experimental result of relevant test.

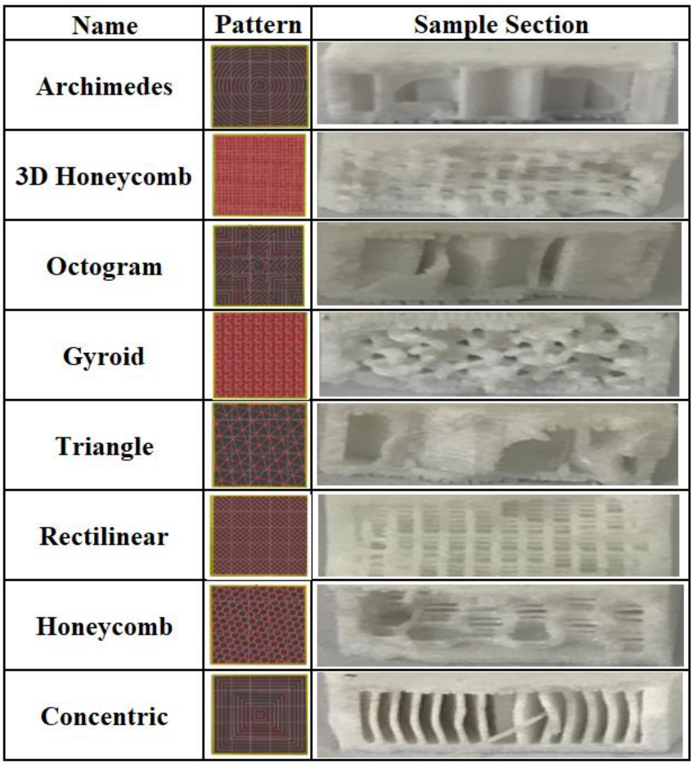

Figure 4.1 Used infill patterns [59]

4.1 Tensile Characteristics

The findings such as stress-strain diagrams, tensile strength, and modulus obtained from the samples with a 20% infill ratio were given in Figure 4.2 according to examined various infill patterns. When looking at the stress-strain diagrams (Figure 4.2(a)), the highest value of ultimate tensile strength (UTS) and the highest elastic region was achieved from the Concentric pattern, and the lowest ones were obtained from the Triangular pattern. Because in the fracture section, the Triangle pattern was the pattern containing the most gaps, while the Concentric pattern was fuller parallel to the fracture direction. While the maximum tensile strength was recorded as 19.33 MPa with a maximum load of 1985.09 N, the minimum value was seen as 13.77 MPa under the load of 1424.59 N. Additionally, the tensile strength values of other patterns, as shown in Figure 4.2(b), were found as 18.12 MPa, 17.22 MPa, 15.4 MPa, 15.29 MPa, 15.03 MPa, 14,29 MPa for Rectilinear, 3D Honeycomb, Octogram, Archimedes, Gyroid, Honeycomb, respectively. As seen in Figure 4.2(c), tensile modulus results except the Triangular pattern showed a similar trend with tensile strength results. The maximum tensile modulus as 827.4 MPa was obtained from the Concentric pattern based on the highest strength and load, which was 32.5% higher than the Gyroid pattern (624.48 MPa). Similarly, Pandzic et al. [50] and Dezaki et al. [49] found the Concentric pattern showed the highest tensile strength and yield strength compared to other models for PLA filament with a %90 infill ratio.

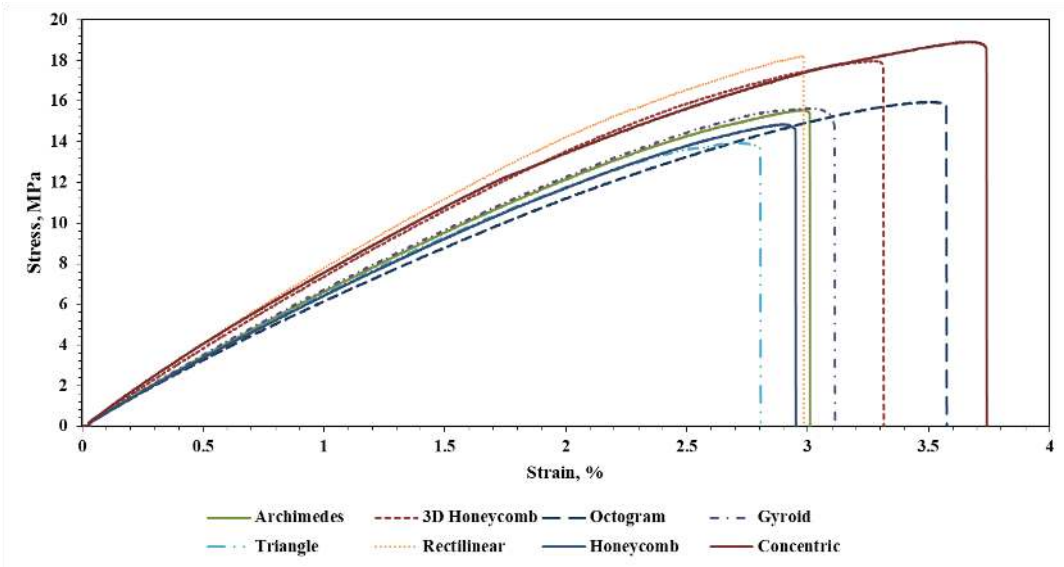

(a)

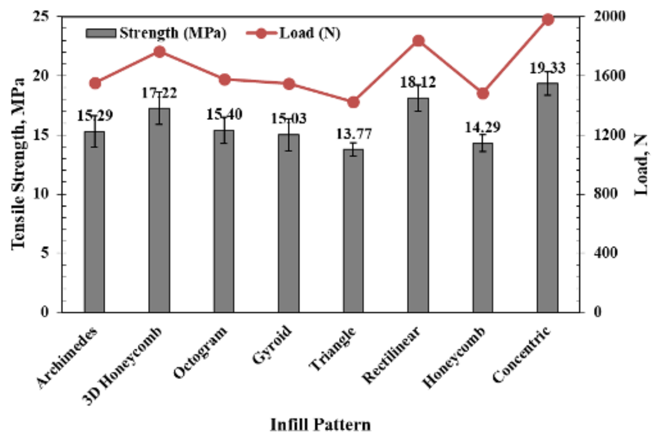

(b)

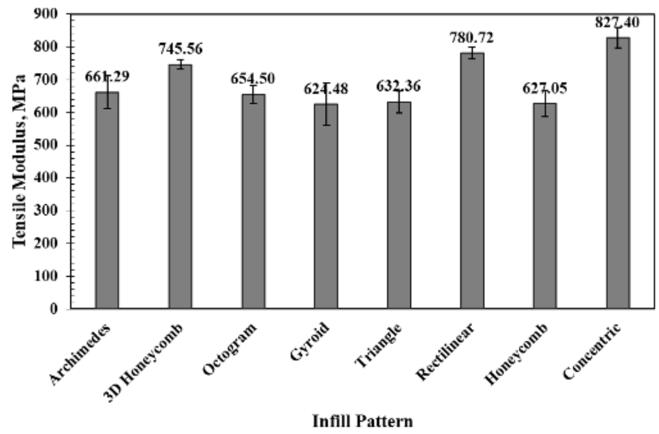

(c)

Figure 4.2 The samples with 20% infill ratio; (a) Stress-strain diagrams, (b) Tensile strength and maximum load, (c) Tensile modulus

All damaged samples with a 20% infill ratio were presented in Table 4.1. When fracture sections of the samples with different infill patterns were examined, the gap seen in the Triangle pattern was more than the others. This can be attributed to the less load-bearing capability of the Triangle pattern due to the more brittle behavior causing more catastrophic failure in the tensile loading. However, the Concentric pattern exhibited more ductile characteristics thanks to the threads printed in the same direction as the tension direction, which contributed to the resistance against applied loads. Likewise, the Rectilinear pattern was also showed a good performance by withstanding the high load and strength due to the way it is printed parallel to the drawing direction. The reason why Concentric behaved better than Rectilinear was thought to be the thinner structure of the Rectilinear lattice. The breaks in 20% infill ratio occurred in mid-region for the Concentric, Archimedes, Rectilinear, Gyroid, and

Octogram patterns. On the other hand, the Honeycomb, Triangle, 3D Honeycomb patterns showed the breakages outside the center of the samples.

Table 4.1 Damaged samples with 20% infill ratio after the tensile experiment

Pattern	Tensile Samples with 20% Infill Ratio	Section
Archimedes		
3D Honeycomb		
Octogram		
Gyroid		
Triangle		
Rectilinear		
Honeycomb		
Concentric		

The stress-strain graphs, tensile strength, and tensile modulus values of the samples having a 40% infill ratio and different infill patterns were shown in Figure 4.3. The area under curves was the biggest for the Concentric pattern which showed the best performance among the examined patterns. Here, the Gyroid samples exhibiting the more ductile behavior showed the highest elongation at break (4.18%) which was the latest than others. On the contrary, Archimedes having one of the lowest load-carrying capacity showed earlier failures than others. Differently from the results of the samples with a 20% infill ratio, Archimedes and Octogram patterns had lower tensile strength and tensile modulus than the Triangle pattern. The maximum tensile strength was seen as 27.48 MPa (Concentric) which was 68.17% higher than the Octogram pattern (16.34 MPa). In addition, the tensile strength of other patterns was recorded as 22.98 MPa, 22.89 MPa, 22.09 MPa, 18.61 MPa, 16.84 MPa, 16.68 MPa for 3D Honeycomb, Rectilinear, Honeycomb, Gyroid, Triangle, Archimedes, respectively.

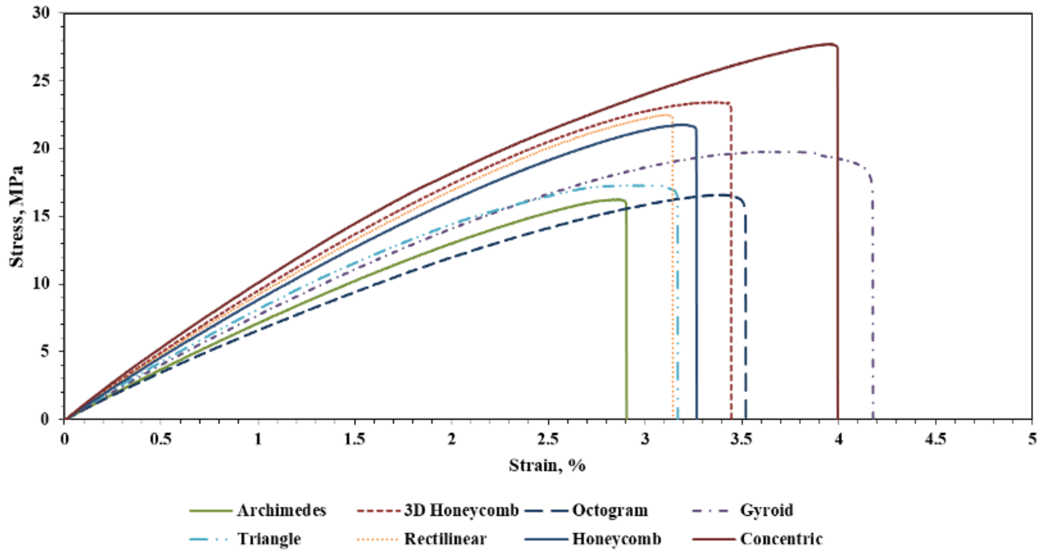

(a)

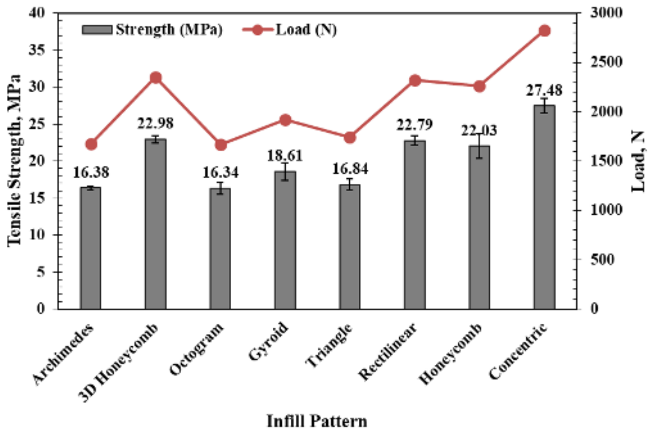

(b)

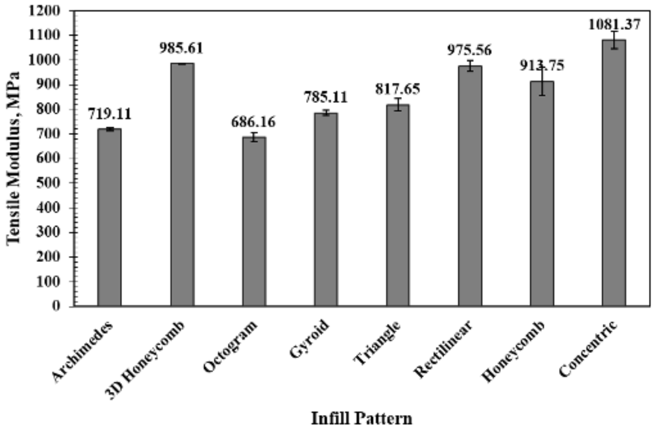

(c)

Figure 4.3 The samples with 40% infill ratio; (a) Stress-strain diagrams, (b) Tensile strength and maximum load, (c) Tensile modulus

The damaged samples with a 40% infill ratio for different infill patterns were presented in Table 4.2. When the refractions were examined, except for Honeycomb, 3D

Honeycomb, and Rectilinear patterns, other patterns were broken in the middle. In the sample having the concentric pattern, it was broken from both the right and the left near the support points, and the beginning of cracking occurred in the middle part. The Gyroid pattern, which was the most ductile material, showed a cross-breaking in the section. Compared to the samples with 20% infill ratio, it was observed that as the filling ratio increased, the tensile strength increased and the visible gap decreased further in the Triangle pattern.

Table 4.2 Damaged samples with 40% infill ratio after the tensile experiment

Pattern	Tensile Samples with 40% Infill Ratio	Section
Archimedes		
3D Honeycomb		
Octogram		
Gyroid		
Triangle		
Rectilinear		
Honeycomb		
Concentric		

The obtained diagrams and results belonging to the samples having a 60% infill ratio were presented in Figure 4.4. The Concentric patterns as seen in previous infill ratios exhibited the highest load-bearing capability. Furthermore, it showed the highest elongation at a break of 4.47%. In general, it can be said that as the infill ratio increased, the elongation was getting high due to the material density. The maximum tensile strength of 35.47 MPa was obtained from the Concentric while the minimum one as 16.34 MPa was achieved from the Octogram pattern. Other patterns showed the tensile strength of 26.41 MPa, 25.84 MPa, 25.54 MPa, 21.66 MPa, 18.71 MPa, 16.88 MPa for 3D Honeycomb, Rectilinear, Honeycomb, Gyroid, Triangle, Archimedes, respectively. The pattern of 3D Honeycomb exhibiting the higher load-bearing capability and lower elongation showed more brittle behaviors compared to other patterns. Similar trends were obtained with tensile strength in the tensile modulus results. The maximum module was seen as 1361.52 MPa (Concentric).

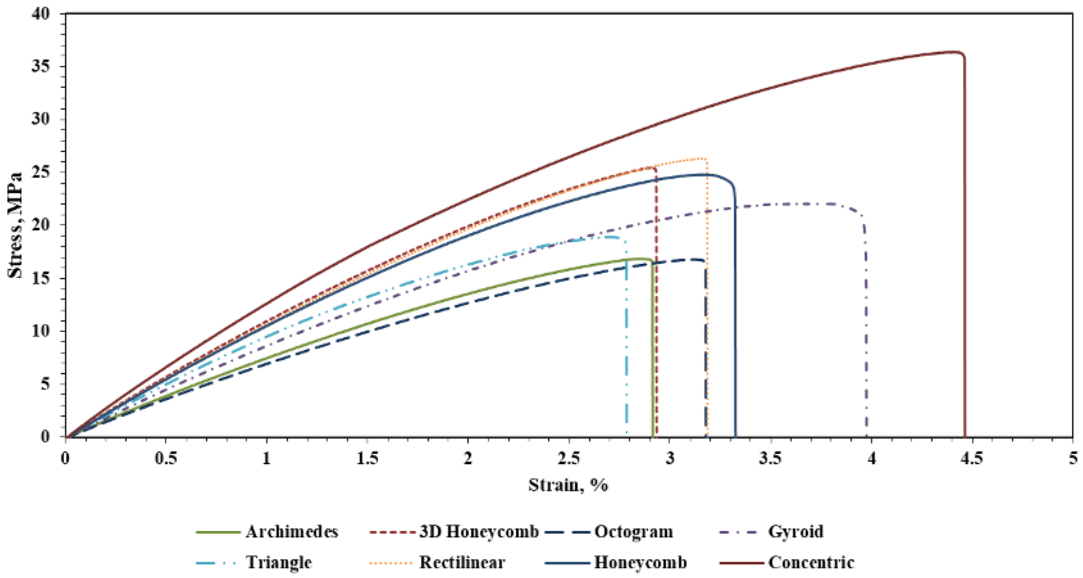

(a)

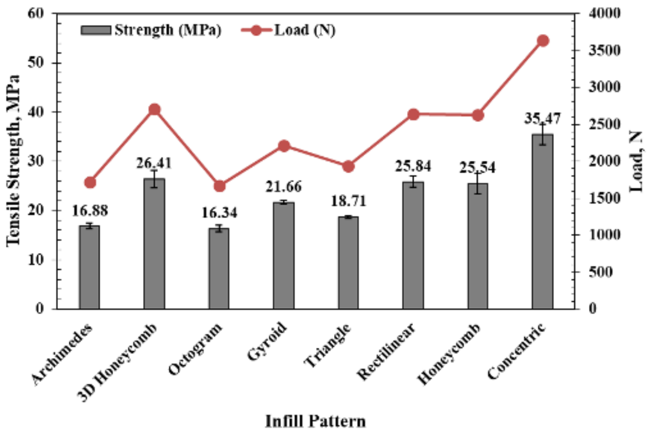

(b)

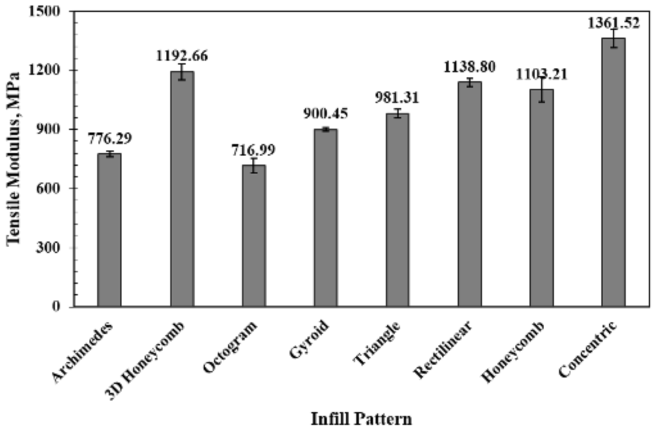

(c)

Figure 4.4 The samples with 60% infill ratio; (a) Stress-strain diagrams, (b) Tensile strength and maximum load, (c) Tensile modulus

The failures of the samples were shown in Table 4.3. In general, the brittle failures were seen due to the normal stress concentrations. However, the Concentric pattern exhibited more catastrophic breakages due to the higher load-carrying capacity. On the right side of Table 4.3, it can be clearly seen that the infill ratio was getting higher than previous configurations. According to the infill pattern, the failure of plastic joints which was seen between each pattern was the main responsible for each sample failure.

Table 4.3 Damaged samples with 60% infill ratio after the tensile experiment

Pattern	Tensile Samples with 60% Infill Ratio	Section
Archimedes		
3D Honeycomb		
Octogram		
Gyroid		
Triangle		
Rectilinear		
Honeycomb		
Concentric		

The tensile characteristics of the samples with different infill patterns at 80% infill ratio were shown in Figure 4.5. The properties in terms of stress-strain diagrams, tensile strength, and tensile modulus were given in Figures 4.5(a)-to 4.5(c), respectively. It can be said that the toughness of the Concentric samples had the highest amongst the examined patterns because it showed the biggest area under stress-strain curves. However, the Gyroid pattern showed much more elongations (4.68%) compared to others. Additionally, the Archimedes exhibited the lowest load-bearing capability. The maximum tensile strength of 39.26 MPa was again obtained from the Concentric patterns. This was 135.65%, 18.00%, 109.72%, 44.02%, 72.80%, 18.04% and 30.82% higher than the Archimedes (16.66 MPa), 3D Honeycomb (33.27 MPa), Octogram (18.72 MPa), Gyroid (27.26 MPa), Triangle (22.72 MPa), Rectilinear (33.26 MPa) and Honeycomb (30.01 MPa), respectively.

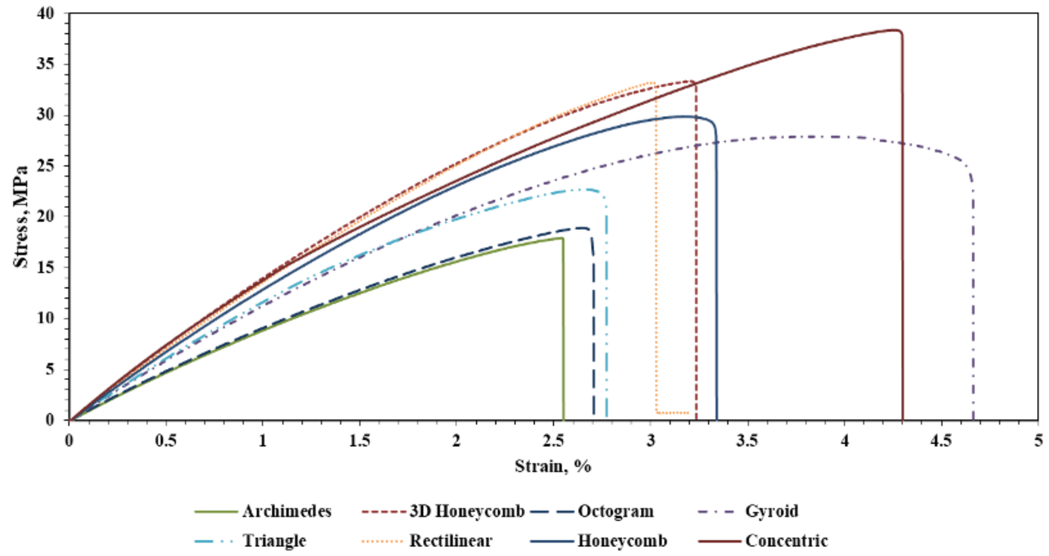

(a)

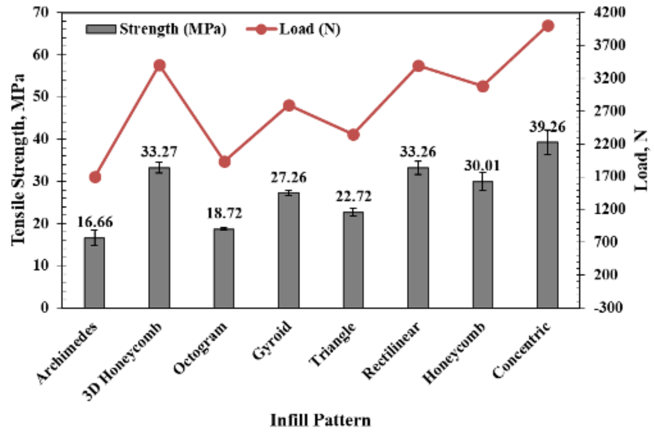

(b)

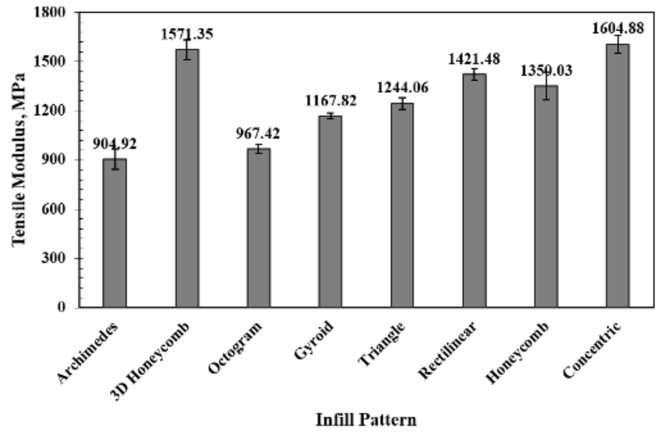

(c)

Figure 4.5 The samples with 80% infill ratio; (a) Stress-strain diagrams, (b) Tensile strength and maximum load, (c) Tensile modulus

The damaged samples with an 80% infill ratio and different infill patterns were presented in Table 4.4. Similarly, with previous failure views, the most catastrophic failures were observed for the Concentric pattern due to its higher load-bearing capability. As the infill ratio increased, the unit gaps in the sections decreased as seen in Table 4.3 and Table 4.4. While these made the material stronger mechanically, it provided that it reached a more brittle structure. However, as the infill ratio increased, parameters such as material amount and printing time could be negatively affected.

Table 4.4 Damaged samples with 80% infill ratio after the tensile experiment

Pattern	Tensile Samples with 80% Infill Ratio	Section
Archimedes		
3D Honeycomb		
Octogram		
Gyroid		
Triangle		
Rectilinear		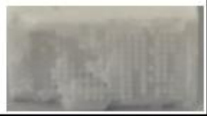
Honeycomb		
Concentric		

Only four different patterns as Archimedes, Octogram, Rectilinear, and Concentric were manufactured as 100% infill ratio by the printer used in material productions. The other patterns were not suitable for printing on the Prusa Mini device with a 100%

infill ratio. The tensile test results obtained from those infill patterns were shown in Figure 4.6. The highest tensile strength (49.82 MPa) and load-carrying capacity (5051.38 N) were obtained from the Concentric pattern, which showed the 4.35% elongation. However, the minimum tensile strength was 20 MPa which was seen for Archimedes pattern. The highest strength results after the Concentric pattern were 42.79 MPa for the Rectilinear and 32.44 MPa for the Octogram, respectively. Compared to previous infill ratios, it was seen that the maximum values in terms of tensile and tensile modulus were obtained from the samples with 100% infill ratios. Similarly, Pandzic et al. [50] stated that it had to print with 100% infill for maximum tensile properties.

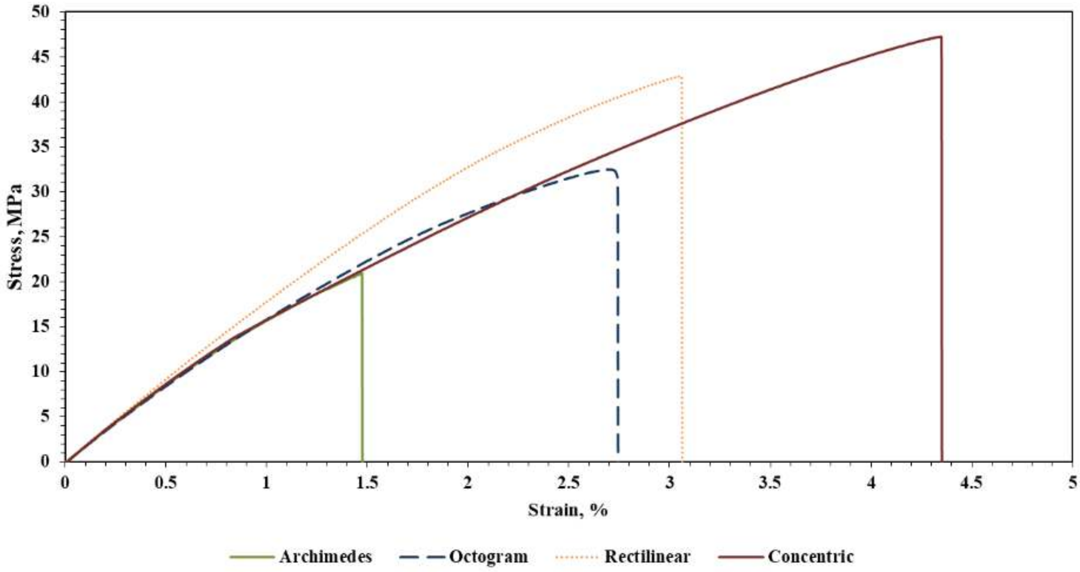

(a)

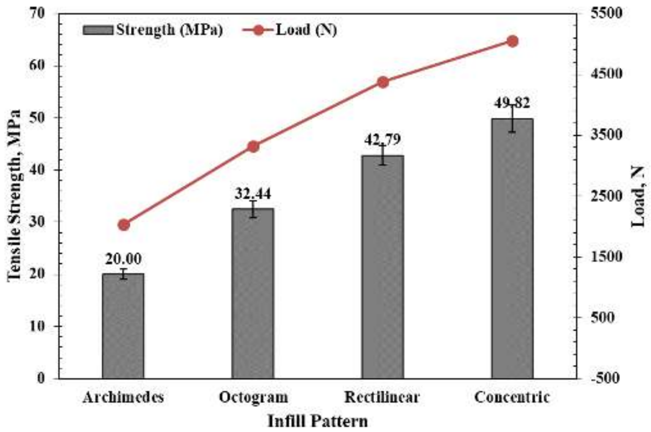

(b)

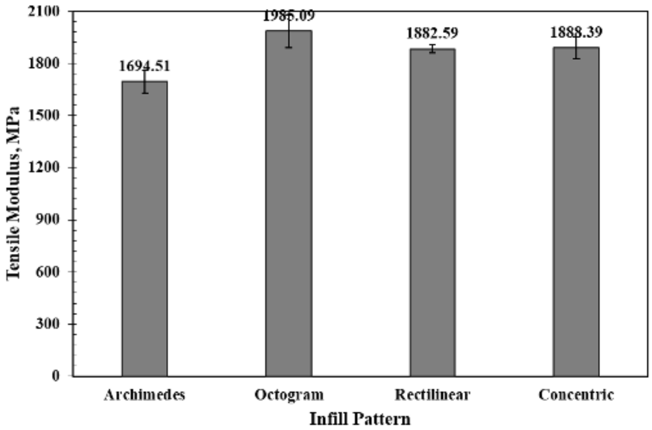

(c)

Figure 4.6 The samples with 100% infill ratio; (a) Stress-strain diagrams, (b) Tensile strength and maximum load, (c) Tensile modulus

According to different infill patterns, the damaged samples with 100% infill ratio were shown in Table 4.5. The most catastrophic failures were seen in the Octogram patterns. In addition, it was divided into 3 parts in total, except for the 20% infill ratio, all breaks were formed in the areas close to the support points.

Table 4.5 Damaged samples with 100% ınfill ratio after the tensile experiment

Pattern	Tensile Samples with 100% Infill Ratio	Section
Archimedes		
Octogram		
Rectilinear		
Concentric		

4.2 Flexural Characteristics

Secondly, to determine the mechanical performance, a test called the flexural test was performed. In the mentioned infill ratios and infill patterns, the specimens were fixed at the edges and subjected to the bending test by applying a certain amount of load from their midpoints. As a result, load-displacement, flexural strength-load, and flexural strains of all samples were examined. When the fractured sections were examined in the evaluations, it was seen that the infill ratio and the pattern greatly affected the mechanical properties.

The findings from the three-point bending experiments for the samples with a 20% infill ratio were presented in Figure 4.7. As similar to tensile test results, the Concentric pattern exhibiting higher resistance to withstand flexural loads showed the better load-bearing capability compared to others. In addition, maximum flexural strength values were obtained from the patterns of Concentric, Rectilinear, and Triangle. While the 3D Honeycomb showed a remarkable performance against tensile loading, it exhibited the worst behavior in terms of load-carrying, flexural strength and modulus. Furthermore, it had the most ductile response in all patterns. The maximum flexural modulus as 1270.29 MPa was achieved from the Concentric pattern.

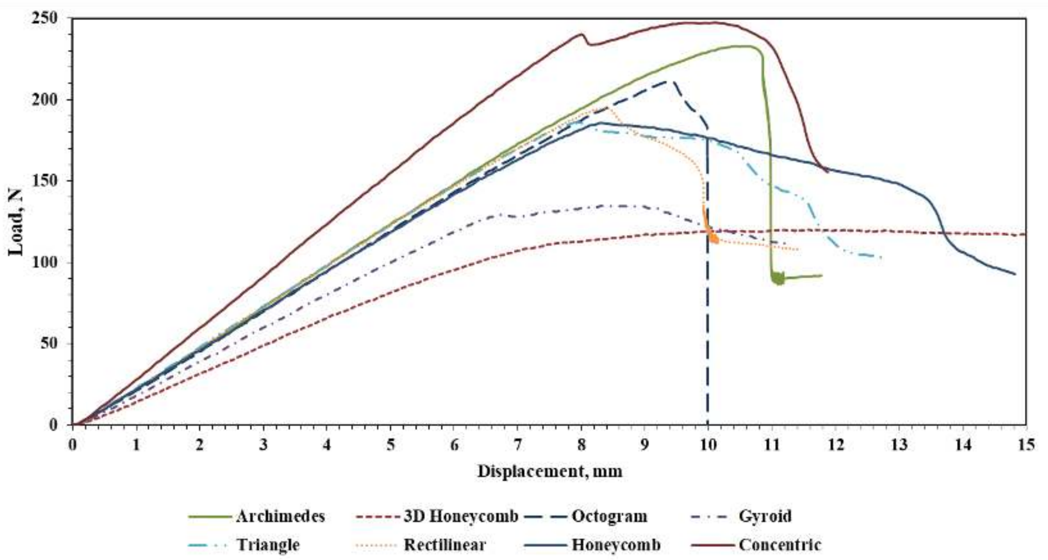

(a)

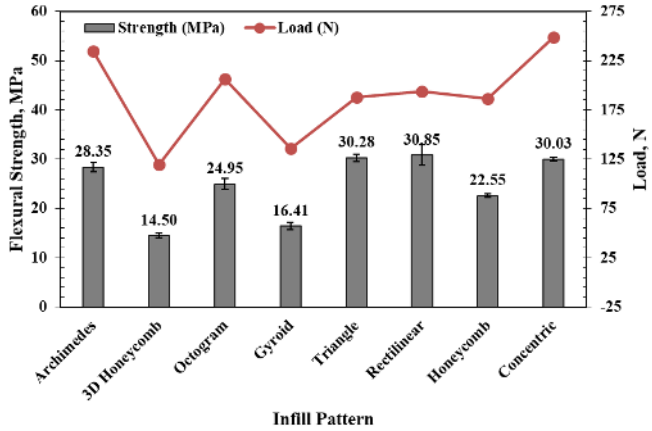

(b)

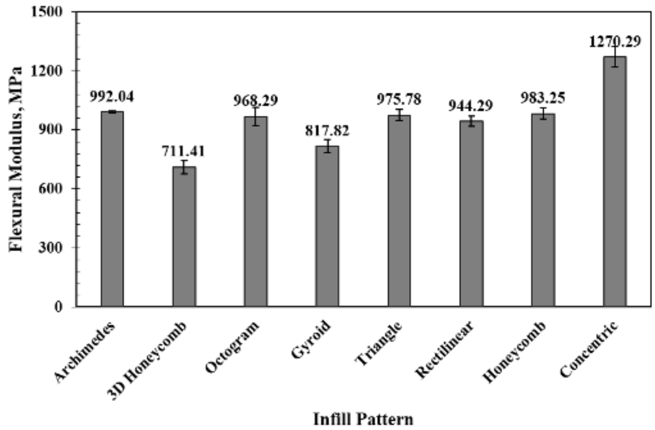

(c)

Figure 4.7 The samples with 20% infill ratio; (a) Load-displacement curves, (b) Flexural strength and maximum load, (c) Flexural strain

The damaged samples with a 20% infill ratio after the flexural test were shown in Table 4.6. The fracture regions showed that the most destructive failures took place in the 3D Honeycomb sample which exhibits the lowest characteristics in strength. However, the Concentric patterns completed its failure process with small separations. The Octogram patterns exhibiting the fracture entire the thickness direction of the samples had more brittle characteristics compared to others.

Table 4.6 Damaged samples with 20% infill ratio after the flexural experiment

Pattern	Flexural Samples with 20% Infill Ratio	Microscopic View
Archimedes	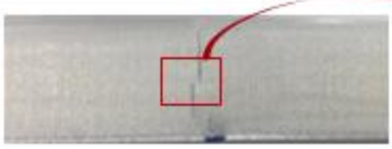	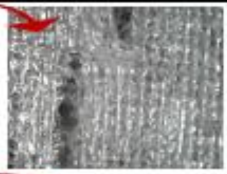
3D Honeycomb	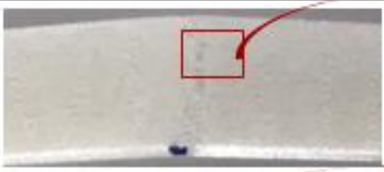	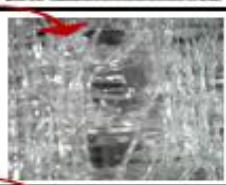
Octogram	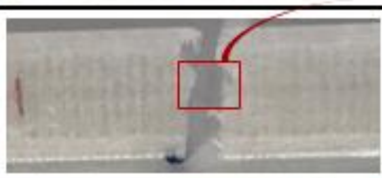	
Gyroid		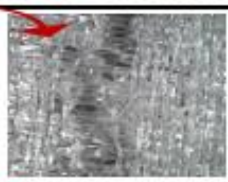
Triangle		
Rectilinear	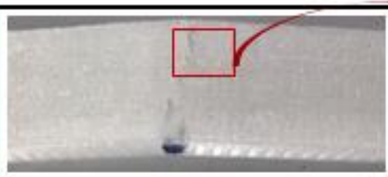	
Honeycomb	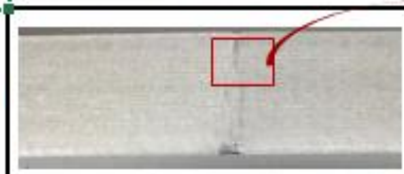	
Concentric		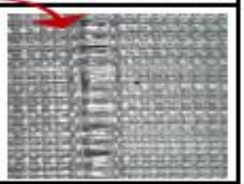

The flexural test results of each pattern having a 40% infill ratio were represented in Figure 4.8. When flexural tests at 40% infill ratio were examined, it is seen that the most ductile material was the Archimedes and secondly Honeycomb. Maximum flexural strength and flexural modulus were obtained from the Concentric pattern again with 44.06 MPa and 1563 MPa under a maximum load of 356.82 N, respectively. Flexural strengths were seen as 43.66, 40.46, 39.63, 37.37, 37.11, 33.72 MPa for the Honeycomb, 3D Honeycomb, Rectilinear, Gyroid, Triangle, Octogram patterns, respectively. The minimum flexural strength and minimum flexural modulus were obtained from the Archimedes pattern.

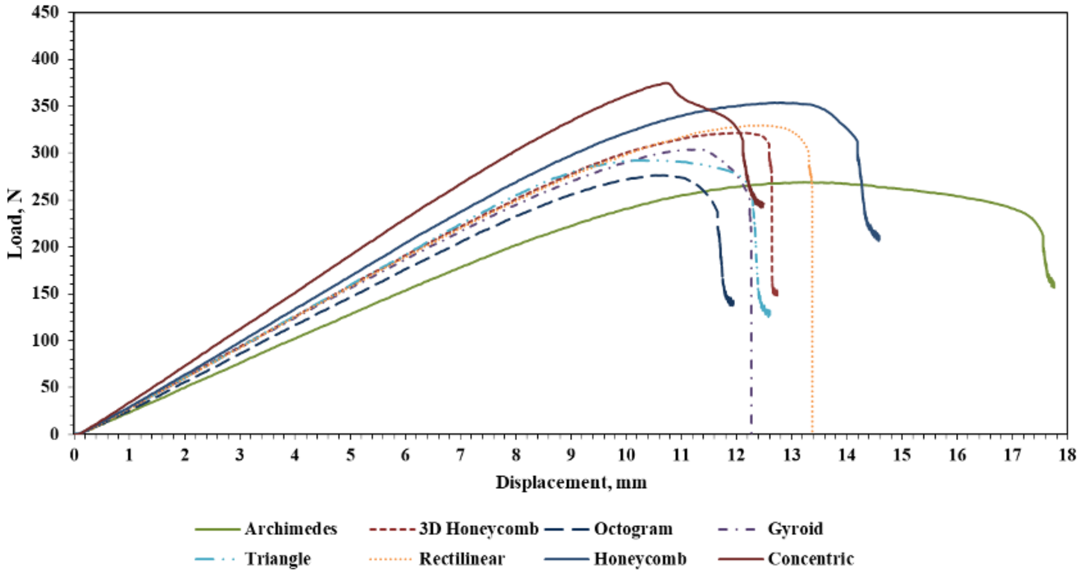

(a)

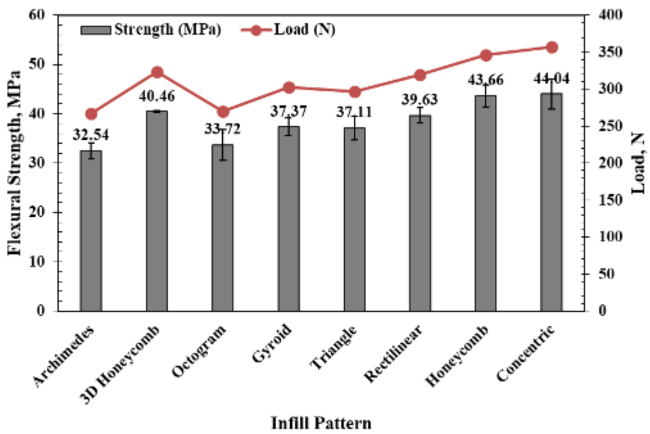

(b)

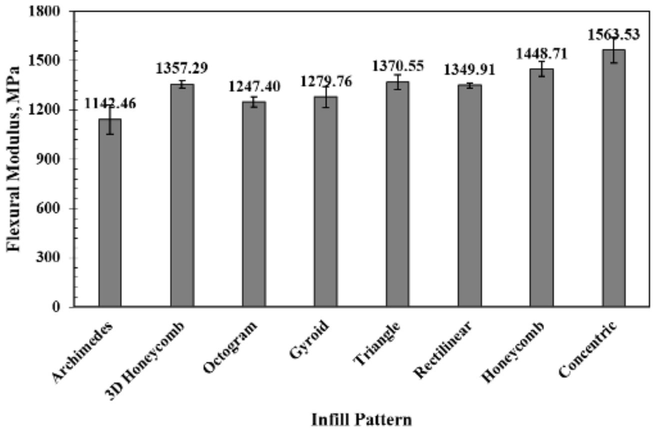

(c)

Figure 4.8 The samples with 40% infill ratio; (a) Load-displacement curves, (b) Flexural strength and maximum load, (c) Flexural strain

The damaged views of the samples with a 40% infill ratio was shown in Table 4.7. As similar to 20% damaged samples, the separation of plastic joints of each pattern was clearly seen. Hereby, the Concentric pattern exhibiting the higher resistance to loads showed less damages compared to others.

Table 4.7 Damaged samples with 40% infill ratio after the flexural experiment

Pattern	Flexural Samples with 40% Infill Ratio	Microscopic View
Archimedes	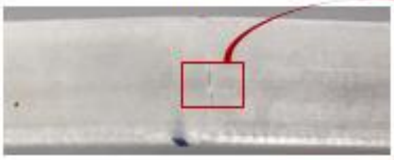	
3D Honeycomb		
Octogram	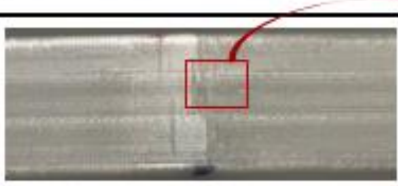	
Gyroid		
Triangle		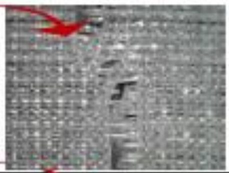
Rectilinear	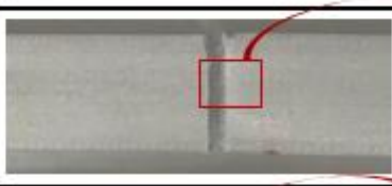	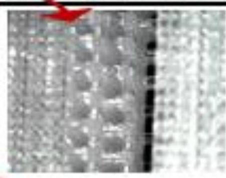
Honeycomb		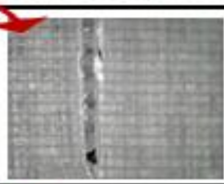
Concentric	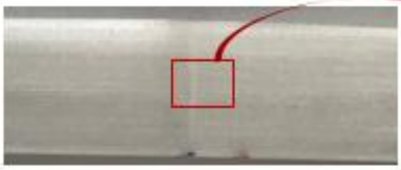	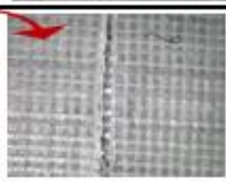

The results of the samples with a 60% infill ratio and different infill patterns obtained from the flexural tests were presented in Figure 4.9. The maximum flexural strength and the maximum flexural modulus as 58.81 MPa and 1777 MPa, respectively, were obtained from the Concentric pattern. Additionally, the minimum tensile strength of

25.48 MPa was obtained from the Octogram pattern which was 56.68% lower than the Concentric pattern.

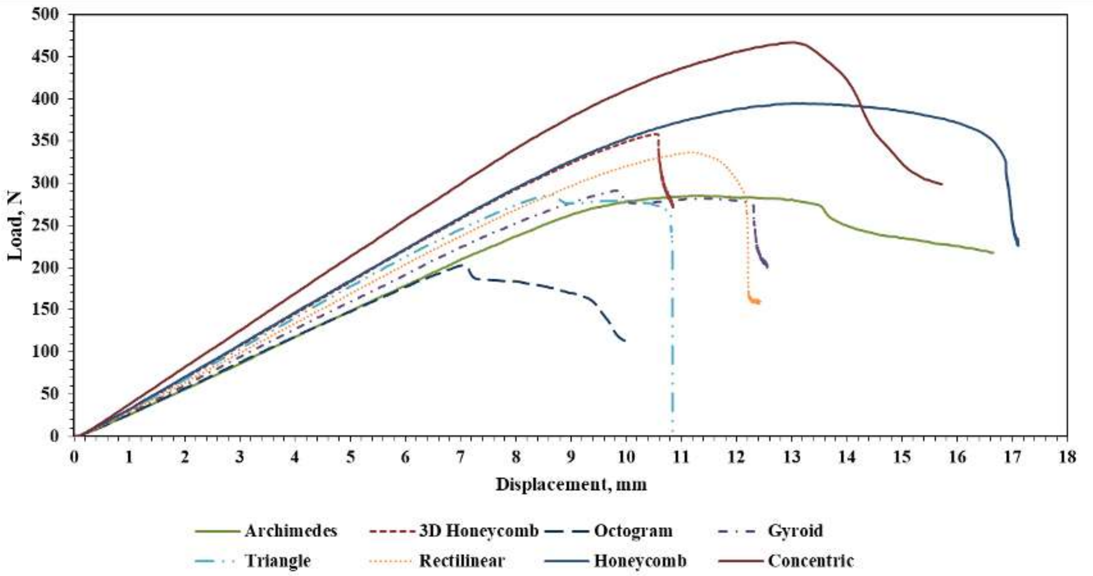

(a)

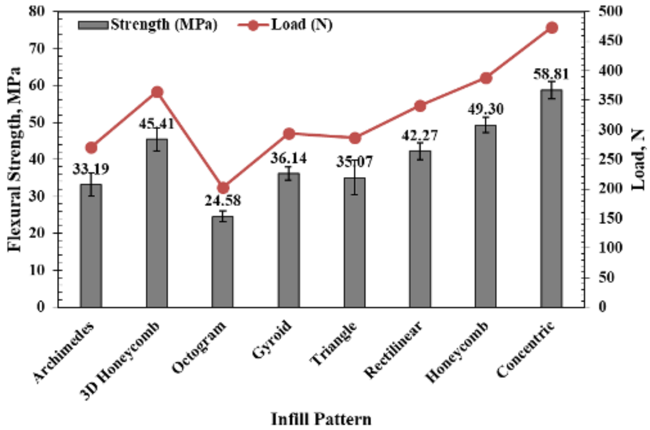

(b)

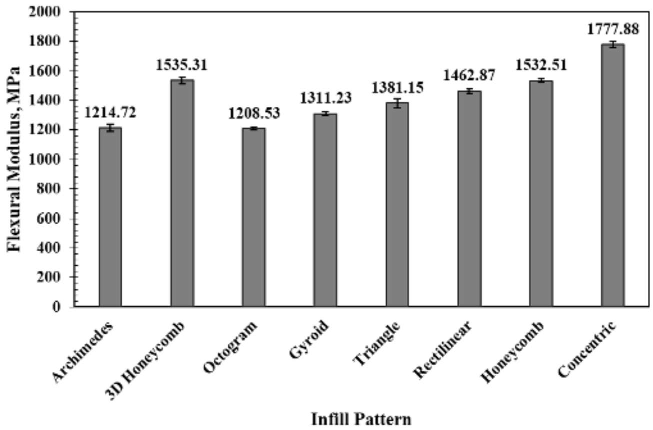

(c)

Figure 4.9 The samples with 60% infill ratio; (a) Load-displacement curves, (b) Flexural strength and maximum load, (c) Flexural strain

The damaged samples with a 60% infill ratio after the flexural experiment were shown in Table 4.8. The plastic joint was failed as a cross in the Triangle and the Octogram patterns while it was seen as regular separations in others. It was observed that the failures were getting more ductile as the material density increased.

Table 4.8 Damaged samples with 60% infill ratio after the flexural experiment

Pattern	Flexural Samples with 60% Infill Ratio	Microscopic View
Archimedes		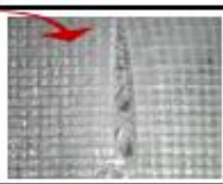
3D Honeycomb	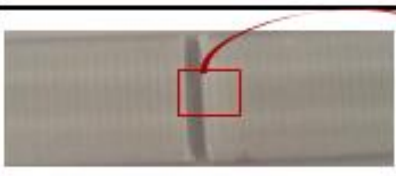	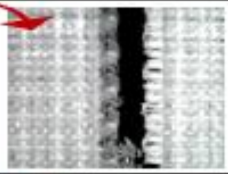
Octogram		
Gyroid	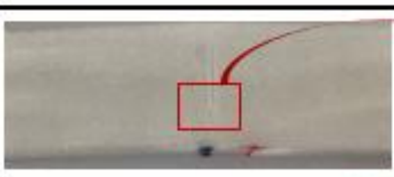	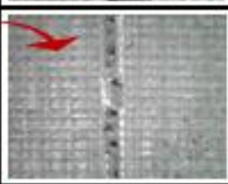
Triangle	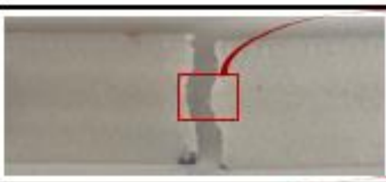	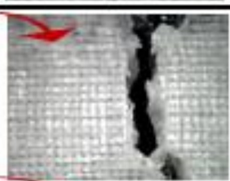
Rectilinear	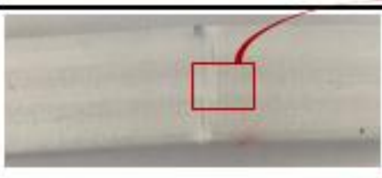	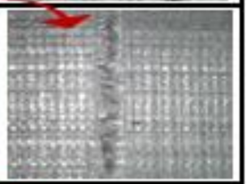
Honeycomb		
Concentric		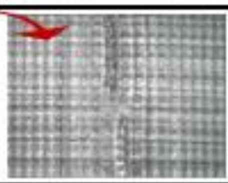

The sample results having an 80% infill ratio were represented in Figure 4.10. The different material responses were observed by the change in infill ratio for all patterns. For example, the Concentric exhibiting the maximum characteristics for load-bearing, strength, and modulus showed more ductile behaviors, unlike previous infill ratios. This can be attributed to the anisotropic nature of PETG thermoplastic filaments. The maximum values of strength and modulus were found as 68.62 MPa and 1954.31 MPa, respectively.

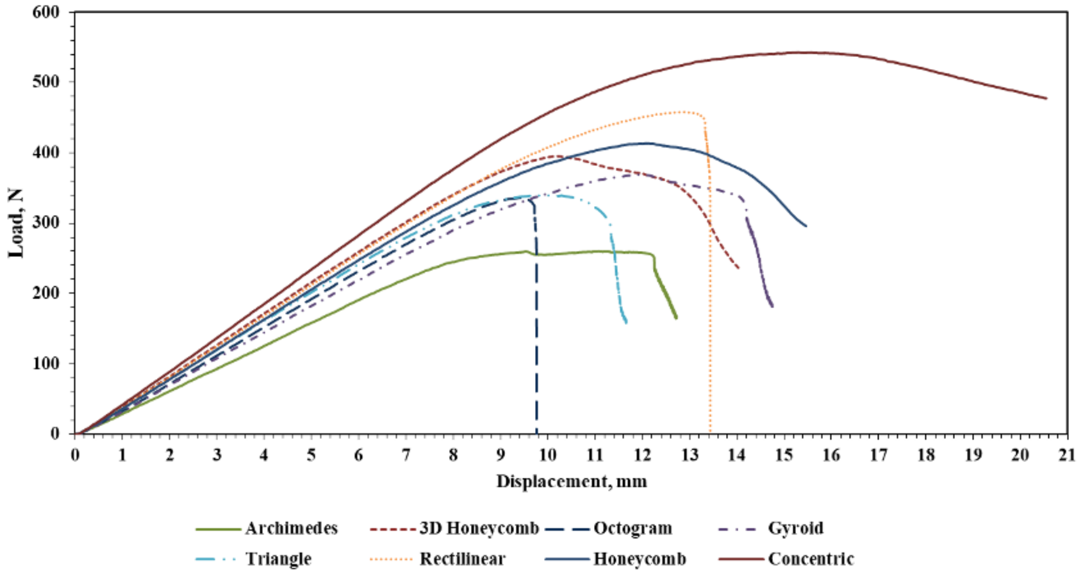

(a)

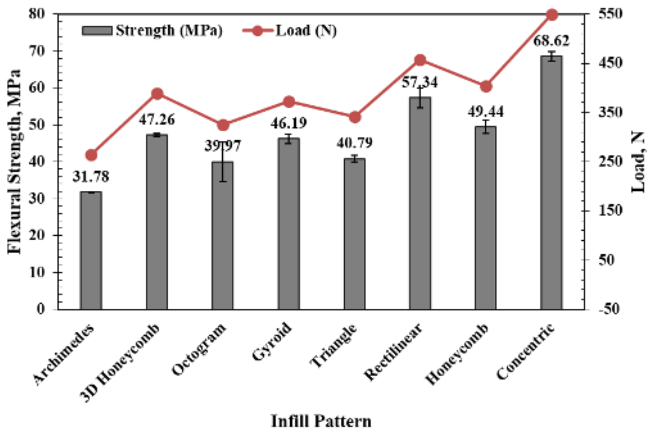

(b)

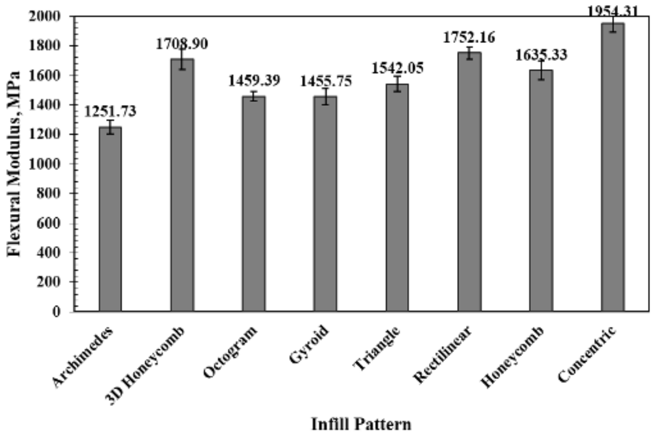

(c)

Figure 4.10 The samples with 80% infill ratio; (a) Load-displacement curves, (b) Flexural strength and maximum load, (c) Flexural strain

The samples having an 80% infill ratio after the flexural experiments were shown in Table 4.9. It can be concluded that the more destructive failures occurred as the infill ratio increased. While the brittle failures were seen in previous infill ratios, here, the shear effects were more dominant for fractures.

Only four patterns were produced at 100% infill ratio which are Archimedes, Octogram, Rectilinear, and Concentric, as seen in Figure 4.11. The highest flexural strength (77.37 MPa) and modulus (2069 MPa) were obtained from the Concentric pattern under maximum load (619.08 N). Secondly, the flexural strength of 60.43 MPa was found from the Rectilinear pattern. While Archimedes showed the lowest values in the previous infill ratio, a remarkable increase was obtained (52.83 MPa). The minimum flexural strength was found as 49.56 MPa and was obtained from the most brittle pattern, the Octogram pattern. Chamil et al. [48] observed that 100% infill ratio had the highest flexural modulus. In addition, they stated the strength of the printed parts decreases as the infill ratio decreases.

Table 4.9 Damaged samples with 80% infill ratio after the flexural experiment

Pattern	Flexural Samples with 80% Infill Ratio	Microscopic View
Archimedes	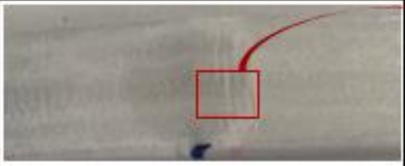	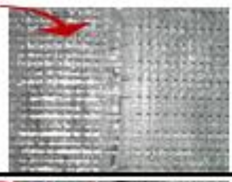
3D Honeycomb	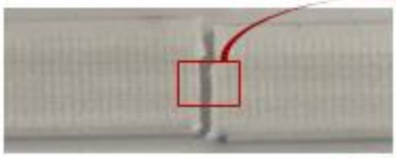	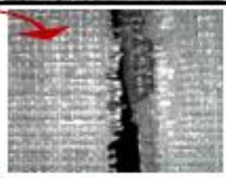
Octogram	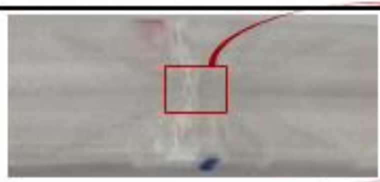	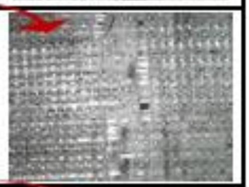
Gyroid		
Triangle	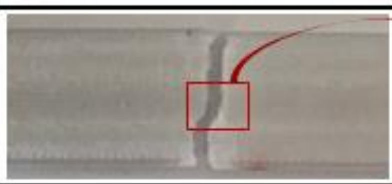	
Rectilinear	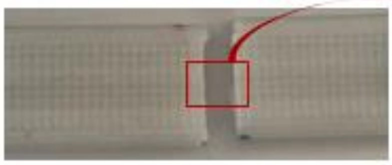	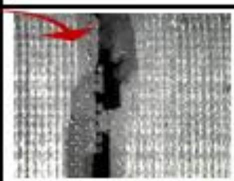
Honeycomb		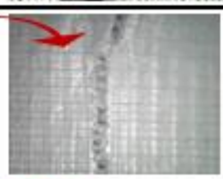
Concentric	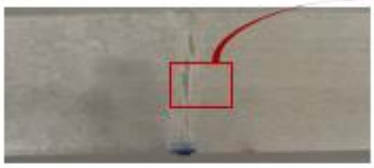	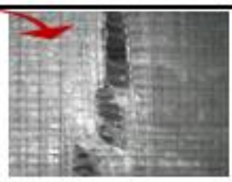

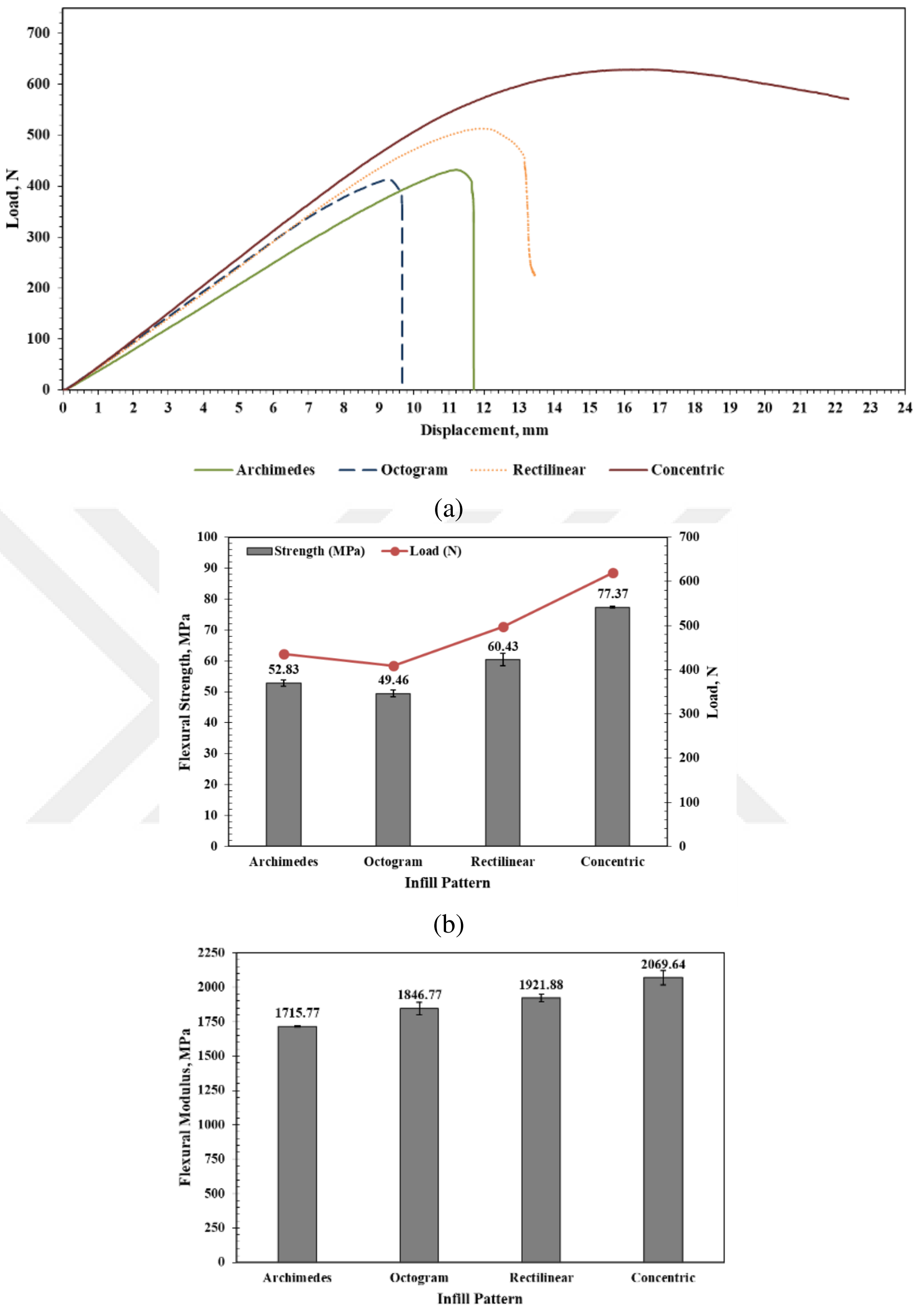

(c)

Figure 4.11 The samples with 100% infill ratio; (a) Load-displacement curves, (b) Flexural strength and maximum load, (c) Flexural strain

The damaged samples with a 100% infill ratio were shown in Table 4.10. The Octogram exhibited a V-type failures due to its pattern geometry. It was concluded that the pattern geometry was a crucial factor for failures of the PETG samples.

Table 4.10 Damaged samples with 100% infill ratio after the flexural experiment

Pattern	Flexural Samples with 100% Infill Ratio	Microscopic View
Archimedes		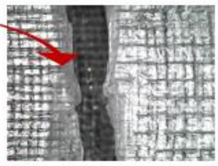
Octogram	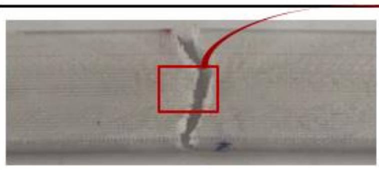	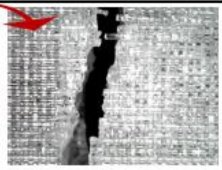
Rectilinear	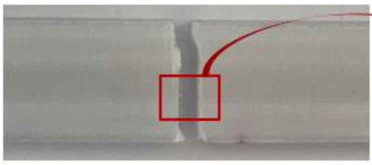	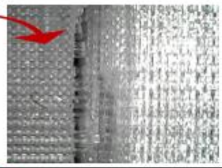
Concentric	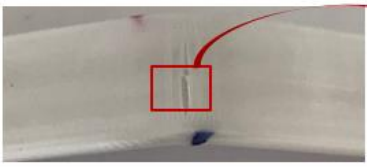	

The flexural strain values for each configuration were seen in Table 4.11. The Concentric pattern showed the highest values for 60%, 80% and 100% infill ratios. However, the Honeycomb and Archimedes had the maximum ones for 40% and 20% infill ratios, respectively. When the deviations were examined, the Archimedes pattern exhibited the highest deviation with 0.45 (40% infill ratio) while the Honeycomb pattern had the lowest deviation of 0.02 (60% infill ratio).

Table 4.11 The flexural strain (%) of the samples

Infill Pattern	Infill Ratio				
	20%	40%	60%	80%	100%
Archimedes	3.16±0.16	3.46±0.45	3.20±0.40	3.20±0.12	3.40±0.10
3D Honeycomb	3.08±0.43	3.35±0.13	3.33±0.43	2.83±0.17	-
Octogram	2.67±0.11	3.02±0.13	2.04±0.04	2.81±0.24	2.75±0.25
Gyroid	2.26±0.14	3.40±0.25	3.31±0.34	3.49±0.16	-
Triangle	1.30±0.10	2.90±0.21	2.56±0.20	3.09±0.18	-
Rectilinear	1.34±0.07	3.45±0.21	3.30±0.32	3.82±0.11	3.28±0.22
Honeycomb	2.38±0.04	3.67±0.05	3.78±0.02	3.79±0.24	-
Concentric	2.92±0.22	3.07±0.25	4.02±0.16	4.36±0.32	4.69±0.05

4.3 Comparison of infill ratios on samples with same infill patterns

The tensile and flexural strength values of the PETG samples fabricated by a 3D Printer using the FDM technique were given in Table 4.12 and Table 4.13, respectively. It can be said that the strength values of each examined pattern were increased with an increment in infill ratios of the samples. The following results can be listed to make comments on the infill ratio effect:

- First of all, 40%-60%-80% infill ratios showed almost the same mechanical behavior in Archimedes' pattern. In fact, the tensile and flexural strengths at 60% infill ratio were higher than 80%. Compared to the others, it had the lowest tensile and flexural strength at an 80% infill ratio. There were circles at the middle region of the Archimedes pattern. The circular pattern of the Archimedes caused high stress concentration in the middle.

Figure 4.12 Section of Archimedes pattern with 60% infill ratio

- When looking at the 3D Honeycomb pattern, an average of 5 MPa tensile strength increased for every 20% infill ratio increased. In the flexural test, when the infill ratio from 20% to 40% increased, it increased almost 3 times, while it increased only 5MPa for 60% and 80% infill ratio.

- In the Octogram pattern, on the other hand, tensile strength remained almost the same at 20%-40%-60%-80% infill ratios, while its strength at 100% infill ratio was 2 times the others. In the flexural test, 60% and 20% infill ratios were the same. It provided twice the flexural strength of 20% density at a 100% infill ratio. At 80% infill ratio, it was the pattern with the worst tensile and flexural behaviors after the Archimedes pattern.

- In the Gyroid pattern, the tensile strength increased by approximately 3 MPa at 20%-40%-60% infill ratios. At 80%, it provided twice the tensile strength of 20%. In flexural strength, the 40% infill ratio was more than 2 times the strength it received at 20%, while the same flexural strength was achieved at 60% and 40%. At 80%, it provided 10 MPa more flexural strength than 60%. Pandzic et al. [50] found that increased infill ratio from 10% to 90%, both ultimate tensile strength for 50% and yield strength for 64% were increased for the "Gyroid" infill pattern for PLA filament.

- In the Triangle pattern, an average of 3 MPa tensile strength increased for each 20% infill ratio increase. In flexural strength, 40% and 60% were almost the same. At 80% infill, it was the pattern that exhibits the worst flexural and pulling behavior after the Archimedes and Octogram patterns. Pandzic et al. [50] stated that, for the "Triangles" infill pattern, with the increase in the infill ratio from 10% to 90%, both ultimate tensile strength for 45% and yield strength for 44% were increased for PLA filament.

- Rectilinear pattern tensile strength showed an increase of approximately 4 MPa at 20%-40% infill ratios and approximately 10 MPa at 60% and 80% infill ratios. It showed maximum tensile and flexural behavior after the Concentric pattern at 100% infill ratios.

- The Honeycomb pattern increased 2 times in flexural strength from 20% to 40% infill pattern, while the increase in other densities was almost nonexistent, although it was the third-best. The tensile strength increased by 2 times of 20% at 80% strength. It was at average levels. Ćwikła et al. [46] stated that have both, a lightweight and durable element, the best set of parameters was the use of a Honeycomb pattern with a infill ratio of about 40-50%.

- In the Concentric pattern, the highest tensile and flexural (except 20% infill in flexural strength) was obtained from it in all infill ratios. It provided an increase of approximately 14 MPa at each infill ratio in flexural strength, and an increase of 7 MPa in tensile strength at each infill ratio. The tensile strength was almost the same only at 60% and 80%. Dezaki et al. [49] and Pandzic et al. [50] found that the "Concentric" pattern exhibited the highest tensile strength and yield strength compared to other models for the PLA and ABS filaments. It can be said that there were fractures 3 pieces at Concentric pattern for all infill ratio except 20%, due to the fact that tensile specimen is dogebone and the pattern near the supports are so weakness. There were parallel to tensile direction of the pattern.

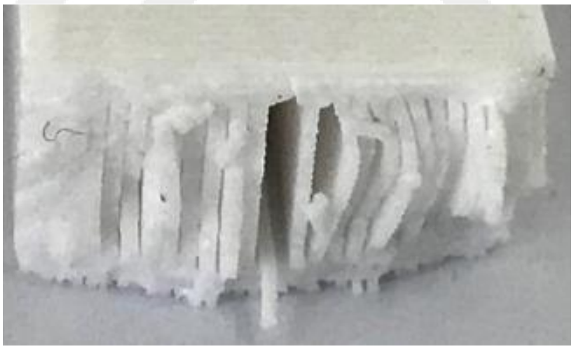

Figure 4.13 Section of Concentric pattern in 80% infill ratio

- Samples showed different tensile strength and different flexural strength for 100% infill ratio. Actually 100% infill ratio means should full completely. However, due to the layered addition in the 3D printer production technique, air gaps occurred for all patterns even if the 100% infill ratio is present.

Table 4.12 Tensile strength (MPa) for different infill ratios

Infill Pattern	Infill Ratio				
	20%	**40%**	**60%**	**80%**	**100%**
Archimedes	15.29	16.38	16.88	16.66	20.00
3D Honeycomb	17.22	22.98	26.41	33.27	-
Octogram	15.40	16.34	16.34	18.72	32.44
Gyroid	15.03	18.61	21.66	27.26	-
Triangle	13.77	16.84	18.71	22.72	-
Rectilinear	18.12	22.79	25.84	33.26	42.79
Honeycomb	14.29	22.03	25.54	30.01	-
Concentric	19.33	27.48	35.47	39.26	49.82

Table 4.13 Flexural strength (MPa) for different infill ratios

Infill Pattern	Infill Ratio				
	20%	**40%**	**60%**	**80%**	**100%**
Archimedes	28.35	32.54	33.19	31.78	52.83
3D Honeycomb	14.50	40.46	45.41	47.26	-
Octogram	24.95	33.72	24.58	39.97	49.46
Gyroid	16.41	37.37	36.14	46.19	-
Triangle	30.28	37.11	35.07	40.79	-
Rectilinear	30.85	39.63	42.27	57.34	60.43
Honeycomb	22.55	43.66	49.30	49.44	-
Concentric	30.03	44.04	58.81	68.62	77.37

CHAPTER V

CONCLUSION

In this study, the effects of 3D Printer production parameters on the mechanical response of part produced using PETG filament were investigated. To this end, the samples with five different infill ratios and eight different infill patterns were manufactured by the Fused Deposition Modelling (FDM) technique. The printed samples were exposed to tensile and flexural loadings to provide a better understanding of the behaviors in different directions. The obtained results can be summarized as follows;

- In the tensile test, the maximum and minimum tensile strength were achieved from the Concentric pattern with 100% infill ratio and the Triangle pattern with 20% infill ratio, respectively. In Concentric patterns, some of the filaments printed parallel to the drawing direction could not be a failure in case of breakage as a result of tensile. This image actually proved that the strength was high. The fracture behavior closest to the Concentric pattern (as can be seen from the fracture section) was obtained from the Rectilinear pattern. The highest tensile strength after Concentric at 20% and 100% infill ratio was obtained from this pattern. When the tensile strengths of 40%, 60% and 80% were examined, it was obtained from the 3D Honeycomb pattern after the Concentric pattern. As the Archimedes pattern infill ratio increased, the increase in tensile strength was less than the others. In fact, the tensile strength at 20% and 100% infill ratios was almost the same.

- In the flexural test, while the highest values was obtained from the Concentric pattern with 100% infill ratio, the 3D Honeycomb pattern showed the lowest values at 20% infill ratio. Similar with tensile results, the best flexural strength was obtained from the Concentric pattern, except for the 20% infill ratio in all patterns. This result showed that the filament placement perpendicular to the bending direction increased the strength in the sample.

- The Rectilinear pattern in tensile strength resistance was also seen in its effect on flexural strength due to filament placement. After the Concentric pattern at 80% and 100% infill ratio, the highest flexural strength was obtained from this pattern due to the flat placement of the filaments.

- Additionally, the increments in infill ratios of almost all samples resulted in remarkable increases due to the material density was getting high as a result of their volume being constant.

In conclusion, it can be suggested that 3D Printer production parameters exhibiting significant influences on the mechanical response of PETG materials should be chosen carefully in the application that may use the materials including thermoplastic filaments.

REFERENCES

[1] Rajkumar Velu, Felix Raspall, Sarat Singamneni (2019). 3D printing technologies and composite materials for structural applications, *Green Composites for Automotive Applications*. **Chapter 8,** 171-190.

[2] Ngo, T.D. Alireza Kashani, Gabriele Imbalzano, Kate T.Q. Nguyen, David Hui (2018). Additive manufacturing (3D printing): A review of materials, methods, applications and challenges. *Composites Part B Engineering*. **143,** 172-196.

[3] Valentina Mazzanti, Lorenzo Malagutti, Francesco Mollica (2019). FDM 3D Printing of Polymers Containing Natural Fillers: A Review of their Mechanical Properties. International Journal of Advanced Research in Mecanical Engineering. **11**, 1094-1116.

[4] ISO/DIS 17296-1 (2015). Additive manufacturing -- General principles. *Part 1: Terminology.*

[5] P. Holzmann, J. Robert, A. Aqeel Breitenecker, Soomro, J. S. Erich, (2017). User entrepreneur business models in 3D printing. *Journal of Manufacturing Technology Management*. **1**, 75-94.

[6] Thomas (2019). 3D printed jellyfish robots created to monitor fragile coral reefs. *3D Printer and 3D Printing News*. Intl: www.3ders.org/articles/20181003-3d-printed-jellyfish-robots-created-to-monitor-fragile-coral-reefs.html, 26.04.2021.

[7] Tess (2017). Indian jewelry brand Isharya unveils ‘Infinite Petals’ 3D printer jewelry collection. *3D Printer and 3D Printing News*. Intl: www.3ders.org/articles/20170412-indian-jewelry-brand-isharya-unveils-infinite-petals-3d-printed-kewelry-collection.html, 26.04.2021.

[8] Thomas (2018). GE Transportation to produce up to 250 3D printed locomotive parts by 2025. *3D Printer and 3D Printing News*. www.3ders.org/articles/20180928-ge-transportation-to-produce-up-to-250-3d-printed-locomotive-parts-by-2025.html, 26.04.2021.

[9] Thomas (2019). Paul G. Allen's Stratolaunch space venture uses 3D printing to develop PGA rocket engine. *3D Printer and 3D Printing News*. Intl: www.3ders.org/articles/20181001-paul-g-allens-stratolaunch-space-venture-uses-3d-printing-to-developpga-rocket-engine.html, 26.04.2021.

[10] David (2018). MX3D to install world's first 3D printed steel bridge over Amsterdam canal. *3D Printer and 3D Printing News*. Intl: www.3ders.org/articles/20180403-mx3d-to-install-worlds-first-3d-printed-steel-bridge-over-amsterdam-canal.html, 26.04.2021.

[11] Steven Schain (2017). Real-World Application of 3D Printing. Article of Autodesk Unıversity.

[12] Aranca. Global Additive Manufacturing Segmentation (2014). Source of Courtsey of Graham Tromans Aranca Analysis Intl: https://www.aranca.com/knowledge-library/blogs-and-opinions/business-research/additive-manufacturing-the-next-industrial-revolution, 31.08.2017.

[13] Wikipedia. 3D Printing Processes (2021). Intl: https://en.wikipedia.org/wiki/3D_printing_processes, 26.09.2021.

[14] H. Bikas, P. Stavropoulos, G. Chryssolouris (2016). Additive manufacturing methods and modelling approaches: a critical review. *Int J Adv Manuf Technol.* **83**, 389–405.

[15] Ming-Hsien Hsueh, Chao-Jung Lai, Shi-Hao Wang, Yu-Shan Zeng, Chia-Hsin Hsieh, Chieh-Yu Pan, Wen-Chen Huang (2021). Effect of Printing Parameters on the Thermal and Mechanical Properties of 3D-Printed PLA and PETG, Using Fused Deposition Modeling. *Article of Polymers.* **13**, 1758.

[16] P.I. Anakhu, C.C. Bolu, A.A. Abioye, G. Onyiagha, H. Boyo, K. Jolayemi, J. Azeta (2018). Innovative Foundry Technology and Material Using Fused

Deposition Modeling and Polylactic Acid Material in Sand Casing. *Article in Archives of Foundry Engineering.* **18**,·65-71.

[17] Sung-Hoon Ahn Michael Montero Dan Odell Shad Roundy, Paul K. Wright (2002). Anisotropic material properties of fused deposition modeling ABS. *Article in Rapid Prototyping.* **8,** 248–257.

[18] Agnes Bagsik, Agnes Bagsik (2019). Mechanical Properties Of Fused Deposition Modeling Parts Manufactured With Ultem*9085. *Article in ANTEC.* 1294-1298.

[19] Peter Anakhu, Cristian Bolu, Abiodun Abioye, Joseph Azeta (2018). Fused Deposition Modeling Printed Patterns for Sand Casting in a Nigerian Foundry: A Review. *International Journal of Applied Engineering Research ISSN 0973-4562.* **13,** 5113-5119.

[20] Sylvain Cailleauxab, Noelia M. Sanchez-Ballestera, Yanis A. Guechea, Bernard Bataillea, Ian Soulairol (2021). Fused Deposition Modeling (FDM), the new asset for the production of tailored medicines. *Journal of Controlled Release.* **330**, 821-841.

[21] L.Li, Q.Sun, C.Bellehumeur, P.Gu (2002). Composite Modeling and Analysis for Fabrication of FDM Prototypes with Locally Controlled Properties. *Journal of Manufacturing Processes.* **4**, 129-141.

[22] Luis Suárez, Manuel Domínguez (2020). Sustainability and environmental impact of fused depositionmodelling (FDM) Technologies. *The International Journal of Advanced Manufacturing Technology.* **106**, 1267–1279.

[23] Alice Melocchi, Marco Uboldi, Matteo Cerea, Anastasia Foppoli, Alessandra Maroni, Saliha Moutaharrik, Luca Palugan, Lucia Zema, Andrea Gazzaniga (2020). A Graphical Review on the Escalation of Fused Deposition Modeling (FDM) 3D Printing in the Pharmaceutical Field. *Journal of Pharmaceutical Sciences.* **109**, 2943-2957.

[24] Kianoush Haghsefat, Kianoush Haghsefat (2020). FDM 3D Printing Technology and Its Fundemental Properties. *6th International Conference on Innovation and Research in Engineering Sciences.*

[25] Aboma Wagari, Hirpa G. Lemu (2018). Influence of 3D Printing FDM Process Parameters on Tensile Property of ULTEM 9085. *14th Global Congress on Manufacturing and Management (GCMM-2018).* **30,** 331–338.

[26] Sanna M. Peltola, Dirk W. Grijpma, Ferry P. W. Melchels, Minna Kellomäki (2008). A review of rapid prototyping techniques for tissue engineering purposes. *Annals of Medicine*. **40**, 268-280.

[27] Sanjay Kumar (2003). Selective Laser Sintering: A Qualitative and Objective Approach. *Literature Review on Modeling and Characterization in JOM.* 43-47.

[28] Prashant K. Jain, Pulak M. Pandey, P. V. M. Rao (2008). Effect of delay time on part strength in selective laser sintering. *The International Journal of Advanced Manufacturing Technology.* **43,** 117**.**

[29] Xometry Europe (2021). Stereolithography (SLA) 3D printing: Technology overview. Xometry Intl: https://xometry.eu/en/stereolithography-sla-3d-printing-technology-overview/, 20.07.2021.

[30] Qiang Yang, Zhongliang Lu, Jiangping Zhou, Kai Miao, Dichen Li (2017). A novel method for improving surface finish of stereolithography apparatus. *The International Journal of Advanced Manufacturing Technology*. **93**, 1537–1544.

[31] Kentaro Hata, Hiroshi Ikeda, Yuki Nagamatsu, Chihiro Masaki, Ryuji Hosokawa, Hiroshi Shimizu (2021). Development of Dental Poly(methyl methacrylate)-Based Resin for Stereolithography Additive Manufacturing. *Special Issue Biomaterials in Medical Applications.* **13***,* 4435-4451

[32] Aytug Kara, Athina Vassiliadou, Baris Ongoren, William Keeble, Richard Hing, Aikaterini Lalatsa, Dolores R. Serrano (2021). Engineering 3D Printed Microfluidic Chips for the Fabrication of Nanomedicines. *Special Issue Advances in Microfluidics for Pharmaceutical Applications.* **13**, 2134-2151.

[33] Ana Grzeszczak, Susanne Lewin, Olle Eriksson, Johan Kreuger, Cecilia Persson (2021). The Potential of Stereolithography for 3D Printing of Synthetic

Trabecular Bone Structures. *Special Issue Additive Manufacturing (AM) of Biomaterials.* **14**, 3712-3729

[34] Jordi Martín-Montal, Jesus Pernas-Sánchez, David Varas (2021). Experimental Characterization Framework for SLA Additive Manufacturing Materials. *Special Issue Mechanical Performance of Polymeric Parts Obtained by Additive Manufacturing.* **13**, 1147-1163.

[35] Stampomatica (2020). PLA vs ABS vs PETG vs TPU vs NYLON? What Is The Difference? Stampomatica Intl: https://stampomatica.com/pla-vs-abs-vs-petg-vs-tpu/, 04.12.2020.

[36] S. Terekhina, T. Tarasova, S. Egorov, L. Guillaumat, M. L. Hattali (2020). On the difference in material structure and fatigue properties of polyamide specimens produced by fused filament fabrication and selective laser sintering. *The International Journal of Advanced Manufacturing Technology.* **111**, 93–107.

[37] Jia-wei Cai, Bai-cheng Zhang, Mao-hang Zhang, Yao-jie Wen, Xuan-hui Qu (2021). Indirect 3D printed ceramic: A literature review. *Journal of Central South University.* **28**, 983–1002.

[38] Z.P.Sun, Y.B.Guo, V.P.W.Shim (2021). Static and dynamic crushing of polymeric lattices fabricated by fused deposition modelling and selective laser sintering – an experimental investigation. *International Journal of Impact Engineering.* 160, 104059

[39] Abishek Kafle, Eric Luis, Raman Silwal, Houwen Matthew Pan, Pratisthit Lal Shrestha, Anil Kumar Bastola (2021). 3D/4D Printing of Polymers: Fused Deposition Modelling (FDM), Selective Laser Sintering (SLS), and Stereolithography (SLA). *Special Issue Advanced Materials in 3D/4D Printing Technology.* **13**, 3101-3138.

[40] Choudhari C. M., Patil V. D. (2016). Product Development and its Comparative Analysis by SLA, SLS and FDM Rapid Prototyping Processes. *IOP Conf. Series: Materials Science and Engineering.* **149**, 12009-12017.

[41] Beibit Zharylkassyn, Asma Perveen, Didier Talamona (2021). Effect of process parameters and materials on the dimensional accuracy of FDM parts. *The scientific committee of the International Conference on Materials, Processing & Characterization.* **44**, 1307-1311.

[42] Marco Leite, João Fernandes, Augusto M. Deus, Luis Reis, Maria Fátima Vaz (2018). Study of the influence of 3d printing parameters on the mechanical properties of PLA. *3rd International Conference on Progress in Additive Manufacturing.*

[43] Veronika M. Miron, Gerhard Bräuer, Sebastian Lämmermann, Zoltan Major (2019). Instrumented Charpy Impact Tests of Additively Manufactured Specimens. *International Symposium on Impact Engineering.* 242-247.

[44] Manav Doshi, Ameya Mahale, Suraj Kumar, Singh Samadhan Deshmukh (2021). Printing parameters and materials affecting mechanical properties of FDM-3D printed Parts: Perspective and prospects. *The 2nd International Conference on Functional Material, Manufacturing and Performances.*

[45] Kapil Chawlaa, Rupinder Singhb, Jaspreet Singh (2021). Investigations on flexural strength of multi-material ABS based composite specimen fabricated through FDM technique. *The scientific committee of the Symposium on Synthesis, Characterization & Processing of Inorganic, bio and nano Materials.*

[46] G. Ćwikła, C. Grabowik, K. Kalinowski, I. Paprocka, P. Ociepka (2017). The influence of printing parameters on selected mechanical properties of FDM/FFF 3D-printed parts. *IOP Conf. Series: Materials Science and Engineering 227.*

[47] Miquel Domingo, J.M. Puigoriol, Andres-Amador Garcia-Granada, Jordi Llumà (2015). Mechanical property characterization and simulation of fused deposition modeling Polycarbonate parts. *Journal of Materials & design, Materials and design.* **83**, 670–677.

[48] Chamil Abeykoon, Pimpisut Sri-Amphorn, Anura Fernando (2019). Optimization of fused deposition modeling parameters for improved PLA and

ABS 3D printed structures. *International Journal of Lightweight Materials and Manufacture*.

[49] Mohammadreza Lalegani Dezaki, Mohd Khairol Anuar Mohd Ariffin, Ahmad Serjouei, Ali Zolfagharian, Saghi Hatami, Mahdi Bodaghi (2021). Influence of Infill Patterns Generated by CAD and FDM 3D Printer on Surface Roughness and Tensile Strength Properties. *Appl. Sci.***11**, 7272-7289.

[50] Adi Pandzic, Damir Hodzic, Aleksa Milovanovic (2019). Effect of infill type and density on tensile properties of PLA material for FDM process. *30th DAAAM International Symposium On Intelligent Manufacturing And Automation.*

[51] TWI. What is PETG? (Everything you need to know) (2022). Intl: https://www.twi-global.com/technical-knowledge/faqs/what-is-petg#Applications, 2022

[52] Wikipedia. Polyethylene terephthalate (2021). Intl: https://en.wikipedia.org /wiki/3D_printing_processes, 30.12.2021.

[53] Filkemp. PETG for 3D Printing / 834Q (2017). Intl: https://s3-eu-west-1. amazonaws.com/robosavvy/datasheets/3D_Printer_Filament_PETG.pdf, 03.20217.

[54] Markerbot. Everything you need to know about PETG 3D Printing (2022). https://www.makerbot.com/stories/engineering/everything-you-need-to-know-about-petg-3d-printing/, 2022.

[55] Falah Hasan Abdalsadah, Faisal Hasan, Qasim Murtaza, Abid Ali Khan (2021). Design and manufacture of a custom ankle–foot orthoses using traditional manufacturing and fused deposition modeling. *Progress in Additive Manufacturing*. **6**, 555–570.

[56] Zainab Raheem (2019). Standard Test Method for Tensile Properties of Plastics. *Decision on Principles for the Development of International Standards, Guides and Recommendations issued by the World Trade Organization Technical Barriers to Trade (TBT) Committee. This standard has been approved for use by agencies of the Department of Defense.*

[57] Zainab Raheem (2019). Standard Test Methods for Flexural Properties of Unreinforced and Reinforced Plastics and Electrical Insulating Materials. *Decision on Principles for the Development of International Standards, Guides and Recommendations issued by the World Trade Organization Technical Barriers to Trade (TBT) Committee. This standard has been approved for use by agencies of the Department of Defense.*

[58] Mirko Kariz, Milan Sernek, Murco Murco Obućina, Manja Kitek Kuzman (2017). Effect of wood content in FDM filament on properties of 3D printed parts. *Materials Today Communications*. **14**.

[59] Giselle Hsiang Loh, Eujin Pei, Joamin Gonzalez-Gutierrez, Mario Monzón (2020). An Overview of Material Extrusion Troubleshooting. *Material Development for Additive Manufacturing and Injection Moulding*. **10**, 4776–4804.

CURRICULUM VITAE (CV)

Personal Information

Name and Surname: Beyza TOKLU

Education

	Graduate School	Year
Master	Gaziantep University, Mechanical Engineering Department	2019-
Bachelor	Gaziantep University, Mechanical Engineering Department	2013-2018
High School	Osmaniye Ahmet Cevdet Paşa Anatolian High School	2010-2013

International Visiting

Period	Visiting Institution
15.11.2021 21.11.2021	Fammecanica Data S.p.A. Pescara/ITALY

International Conferance

1) Samples Produced with PETG Filaments at 20% Infill Ratio in Different Infill Patterns and Bending Properties, (PETG Filamentleri ile %20 Dolgu Oranında Üretilen Numunelerin Farklı Dolgu Desenlerinde Çekme ve Eğilme Özellikleri), The 3rd International Eurasian Conference on Science, Engineering and Technology (EurasianSciEnTech 2021). **83**, 15.12.2018-17.12.2018.

Research And Project

1) TOKLU BEYZA, BOZDANA A. TOLGA (2018). University of Gaziantep, Bachelor Degree Graduation Research, *Usage Area of* TiO_2.

2) TOKLU BEYZA, CULFA GİZEM, AKSOY ALİHSAN (2019). Gaziantep, Lidersan Sağlık & Gıda Ürünleri Inc, Product Design Project, *Production of Disposable Diapers that Cover the Baby in Three Dimensions, Can Stretch in Two Dimensions & Suitable for Full Educational and Usage Function*.

3) BOZKURT ÖMER YAVUZ, TOKLU BEYZA, ÖZBEK ÖZKAN (2021). University of Gaziantep, BAP (MF. YLT.21.12), *Experimental research on the effects of printing parameters on the mechanical behavior of 3D printed parts.*